Available online at www.sciencedirect.com
SCIENCE DIRECT®
Journal of volcanology and geothermal research
ELSEVIER
Journal of Volcanology and Geothermal Research 149 (2006) 263–296
www.elsevier.com/locate/jvolgeores

New multibeam mapping and geochemistry of the 30°–35° S sector, and overview, of southern Kermadec arc volcanism

I.C. Wright [a,*], T.J. Worthington [b], J.A. Gamble [c]

[a] *National Institute of Water and Atmospheric Research (NIWA), P.O. Box 14 901, Wellington, New Zealand*
[b] *Institute of Geosciences, University of Kiel, Germany*
[c] *Department of Geology, National University of Ireland, University College Cork, Cork, Ireland*

Accepted 9 March 2005

Abstract

New multibeam mapping and whole-rock geochemistry establish the first order definition of the modern submarine Kermadec arc between 30° and 35° S. Twenty-two volcanoes with basal diameters >5 km are newly discovered or fully-mapped for the first time; Giggenbach, Macauley, Havre, Haungaroa, Kuiwai, Ngatoroirangi, Sonne, Kibblewhite and Yokosuka. For each large volcano, edifice morphology and structure, surficial deposits, lava fields, distribution of sector collapses, and lava compositions are determined. Macauley and Havre are large silicic intra-oceanic caldera complexes. For both, concentric ridges on the outer flanks are interpreted as recording mega-bedforms associated with pyroclastic density flows and edifice foundering. Other stratovolcanoes reveal complex histories, with repeated cycles of tectonically controlled construction and sector collapse, extensive basaltic flow fields, and the development of summit craters and/or small nested calderas.

Combined with existing data for the southernmost arc segment, we provide an overview of the spatial distribution and magmatic heterogeneity along ~780 km of the Kermadec arc at 30°–36°30′ S. Coincident changes in arc elevation and lava composition define three volcano–tectonic segments. A central deeper segment at 32°20′–34°10′ S has basement elevations of >3200 m water-depth, and relatively simple stratovolcanoes dominated by low-K series, basalt–basaltic andesite. In contrast, the adjoining arc segments have higher basement elevations (typically <2500 m water-depth), multi-vent volcanic centres including caldera complexes, and erupt sub-equal proportions of dacite and basalt–basaltic andesite. The association of silicic magmas with higher basement elevations (and hence thicker crust), coupled with significant inter- and intra-volcano heterogeneity of the silicic lavas, but not the mafic lavas, is interpreted as evidence for dehydration melting of the sub-arc crust. Conversely, the crust beneath the deeper arc segments is thinner, initially cooler, and has not yet reached the thermal requirements for anatexis. Silicic calderas with diameters >3 km coincide with the shallower arc segments. The dominant mode of large caldera formation is interpreted as mass-discharge pyroclastic eruption with syn-eruptive collapse. Hence, the shallower arc segments are characterized by both the generation of volatile-enriched magmas from crustal melting and a

* Corresponding author. Tel.: +64 4 386 0300; fax: +64 4 386 2153.
E-mail address: i.wright@niwa.cri.nz (I.C. Wright).

doi:10.1016/j.jvolgeores.2005.03.021

reduced hydrostatic load, allowing magma vesiculation and fragmentation to initiate and sustain pyroclastic eruptions. Proposed initiation parameters for submarine pyroclastic eruptions are water-depths <1000 m, magmas with 5–6 wt.% water and >70 wt.% SiO_2, and a high discharge rate.

Keywords: Submarine stratovolcanoes; Kermadec arc; intra-oceanic arc; silicic magmatism

1. Introduction

Volcanic arcs have complex magmatic histories that feature elemental recycling from the subducting slab, generation of volatile-rich magmas, and both the thermal evolution and growth of arc crust. Understanding these processes requires, at the very minimum, knowledge of the spatial distribution of volcanism, eruption modes, and compositional heterogeneity of the erupted magma. Although the Kermadec arc has been long recognised as an archetypal intra-oceanic arc–back-arc system (Karig, 1970; Ewart et al., 1977; Cole, 1986), the arc has remained poorly documented primarily due to its submarine character for ~1260 km between 25°54′ and 36°24′ S (Fig. 1). Only between 29°14′ and 31°15′ S is the arc emergent, where the summits and associated eroded stacks of the Raoul, Macauley, Curtis, and L'Esperance volcanoes comprise an area of <35 km^2 (e.g. Lloyd and Nathan, 1981; Smith et al., 1988; Lloyd et al., 1996; Worthington et al., 1999; Smith et al., 2003a). The ~200-km long sector immediately adjacent to New Zealand and south of 35° S is relatively well known, consisting of at least 13 edifices, including basaltic–andesitic stratovolcanoes and silicic calderas (Fig. 2A; Gamble and Wright, 1995; Wright and Gamble, 1999). However, elsewhere only reconnaissance ship-track data (e.g. Ballance et al., 1999; Delteil et al., 2002) and satellite gravity inversions (Ramillien and Wright, 2000) provide any clue to the nature and location of the modern arc.

Using EM300 multibeam data, seafloor photography, and rock dredging, we provide the first definition of Quaternary Kermadec arc volcanism between 30° and 35° S. A total of 22 volcanoes with basal diameters >5 km are mapped, with the thirteen largest described in detail. These data, together with those from south of 35° S, give an overview of the spatial distribution and magmatic heterogeneity along ~780 km of the Kermadec arc at 30°–36°30′ S. Coincident changes in tectonic structure and geochemistry are identified along the arc. We show that silicic volcanism, including caldera formation, is a significant component of Kermadec arc

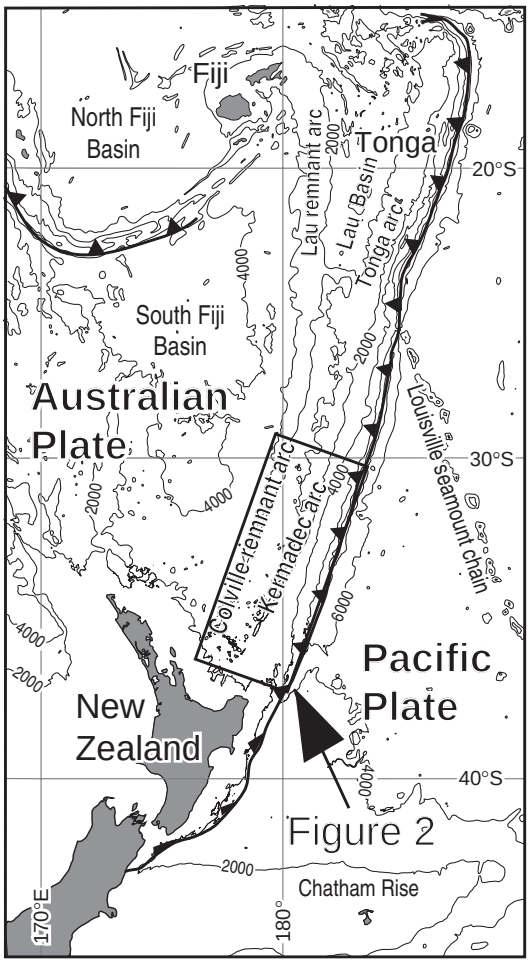

Fig. 1. Regional setting of the Kermadec subduction system and the contiguous Tonga–New Zealand sectors to the north and south, respectively.

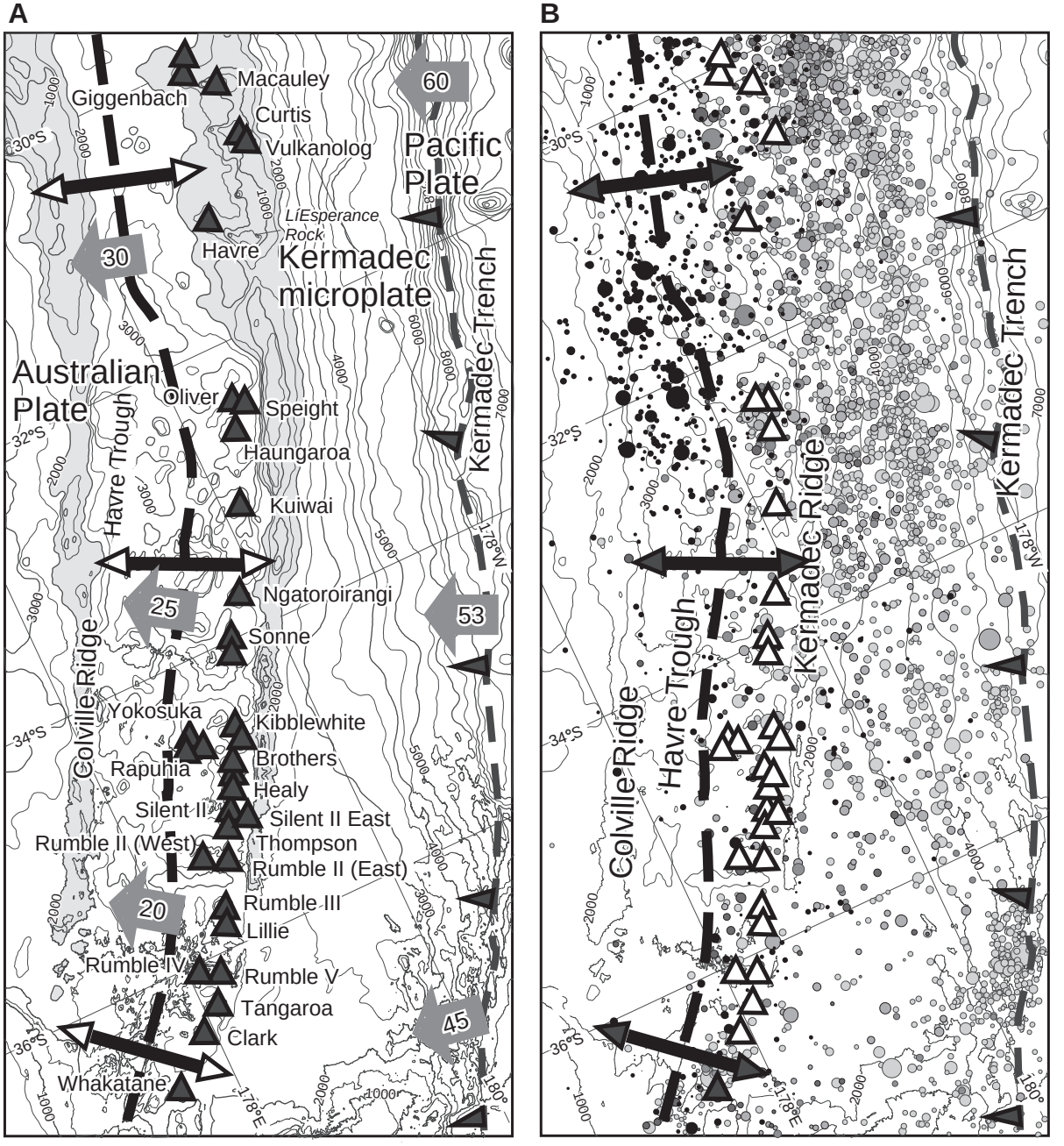

Fig. 2. (A) Regional setting of the southern and central Kermadec subduction system, including newly discovered volcanoes (closed triangles) of the arc front. Dashed lines show location of the subduction and extensional plate boundaries, east and west of the Kermadec microplate, respectively, with grey arrows showing estimated relative PA–KE and KE–AU plate motion in millimeters per annum. (B) Location of southern and central Kermadec arc volcanoes relative to earthquake seismicity (from USGS catalogue, January 1973–April 2003).

volcanism and is spatially related to the more elevated arc segments.

2. Regional setting

2.1. Kermadec subduction system

The contiguous Tonga–Kermadec subduction system primarily involves Pacific (PA)–Australian (AU) plate convergence (Fig. 1), but includes the Niuafo'ou (NF), Tonga (TO) and Kermadec (KE) microplates that accommodate back-arc spreading and rifting in the Lau Basin and Havre Trough (Pelletier and Louat, 1989; Zellmer and Taylor, 2001; Bird, 2003; Ruellan et al., 2003). Along the Kermadec sector, both relative AU–KE and KE–PA motions increase northward (Fig. 2A). The latter is dominant and increases from ~50 mm yr^{-1} at 36° S to 67 mm yr^{-1} at 25° S. Like most other western Pacific subduction zones, the Kermadec system is characterized by subduction of cold and old lithosphere (being >80 Ma at the Kermadec Trench).

Along strike, the Kermadec subduction system (including the trench, volcanic arc, and back-arc region) varies north and south of ~32°30′ S (Pelletier and Dupont, 1990; Ballance et al., 1999). To the north, the remnant Colville Ridge (capped by an extinct Miocene arc) and frontal Kermadec Ridge are wide, the active volcanic arc partially surmounts the frontal ridge, and the Havre Trough back-arc comprises a relatively simple, shallow, and thickly sedimented region (Delteil et al., 2002). To the south, the remnant and frontal ridges are narrower, with the active arc front displaced west of the latter (Wright, 1997), and back-arc comprising a deep and structurally complex region of rifting (Wright et al., 1996). These changes, coupled with the shallower inclination of the subducting slab in the south (Reyners, 1989), progressively increase the trench–arc distance from ~180 km at 30° S to ~220 km at 37° S.

Extension within the back-arc is distributed across the Havre Trough, but includes a series of semi-contiguous, "axial" rift grabens (Caress, 1991; Parson and Wright, 1996; Wright et al., 1996; Delteil et al., 2002). Back-arc rifted fabrics are consistently oblique to the bounding remnant and frontal ridges, and increasingly so to the south (Delteil et al., 2002). Further, the rifted back-arc fabric extends eastward to at least the present-day volcanic arc.

2.2. Kermadec Island volcanism

The volcanic islands of Raoul (Lloyd and Nathan, 1981; Worthington et al., 1999), Macauley (Brothers and Martin, 1970; Lloyd et al., 1996; Smith et al., 2003a), Curtis (Smith et al., 1988) and L'Esperance comprise the emergent summits of large, complex stratovolcanoes formed by coalesced strombolian and phreatomagmatic eruption centres. Strongly porphyritic and vesicular basaltic–andesitic lavas form most of Raoul, Macauley and L'Esperance, whereas Curtis is composed of dacitic pumice. However, dacitic pumice is also widespread on Raoul and Macauley, where recent episodes of voluminous silicic volcanism are associated with caldera formation, pyroclastic flows, and Plinian eruptions with tephra volumes possibly >50 km^3 (Lloyd et al., 1996; Worthington et al., 1999; Smith et al., 2003a). Historical eruptions are recorded only at Raoul, though active fumaroles and hot springs are present on Raoul and Curtis Islands and the submarine flanks of Raoul and Macauley.

Magma genesis varies along the arc. Mafic Kermadec lavas, north of 30° S (and Tonga) require a strongly depleted mantle source fluxed by a hydrous fluid derived mainly from the subducting oceanic crust (Ewart and Hawkesworth, 1987). In contrast, lavas to the south have a less depleted mantle source and an additional contribution from a melt of subducting sediment (Gamble et al., 1996; Turner et al., 1997; Ewart et al., 1998; Haase et al., 2002). Trace element modelling and isotopic homogeneity are broadly consistent with the derivation of silicic magmas by fractional crystallisation of mafic parent bodies (Ewart et al., 1973, 1977), whereas arguments based on relative magma volumes, petrography, changes in silicic magma composition with time at individual volcanoes, and thermal modelling favour a dominant role for crustal anatexis driven by underplating and intrusion of mafic magma (Worthington, 1998; Smith et al., 2003a,b).

2.3. Southernmost Kermadec arc (35°–36°30′ S)

The southernmost arc segment comprises 13 edifices consisting of both basaltic–andesitic stratovolcanoes and silicic caldera complexes (Wright et al., 1996; Wright, 1997; Wright and Gamble, 1999). Of these volcanoes, most basaltic edifices shoal to water-depths <1000 m (and three to <500 m). They record a general

Table 1
Synopsis of location and physical size of southern Kermadec volcanoes south of 30° S, including those between 35° and 36°27′ S for completeness

Volcano	Type	Latitude (°S)	Longitude (°E/°W)	Basal diameter (km)	Summit water-depth (m)	Basal water-depth (m)	Volcano relief (m)	Constructional volume (km^3)
Giggenbach	Stratovolcano/ summit crater	30°02.148′ S	178°42.752′ W	12–18	65	1250	11.71185	35.5
GI1	Satellite cone	30°01.118′ S	178°38.657′ W	4–5	600	1500	900	3.7
GI2	Satellite cone	30°05.935′ S	178°44.672′ W	~8	550	~1400	850	10.3
Macauley	Silicic caldera/ basalt dome-shield	30°12.000′ S	178°29.000′ W	23–30	400	1700	1300	269
	Satellite cone	31°02.850′ S	178°54.300′ W	5–8	800	1600	800	6.3
Havre	Silicic caldera	31°06.500′ S	179°02.450′ W	~25	720	1750	1030	91
Oliver	Satellite cone	32°23.500′ S	179°40.250′ W	7.4	2200	3000	800	7.2
Speight	Satellite cone	32°23.289′ S	179°35.457′ W	5.5	1840	2620	780	13.7
Haungaroa	Stratovolcano/ summit caldera	32°37.000′ S	179°37.422′ W	~31	660	~3100	2440	240.6
Kuiwai	Stratovolcano/ summit craters	33°09.537′ S	179°57.398′ W	~23	560	~3100	2540	157.6
KU1	Satellite cone	33°09.940′ S	179°59.232′ E	3–5	1120	~2100	980	20.9
	Satellite cone	33°24.570′ S	179°52.294′ E	6–12	1100	2750	1650	13.2
Ngatoroirangi	Stratovolcano	33°43.716′ S	179°49.634′ E	25	340	2500	2160	216.6
Sonne	Stratovolcano/ summit calderas	34°04.625′ S	179°34.532′ E	21	995	3000	2005	156
SO1	Satellite cone	34°07.054′ S	179°25.830′ E	7	1640	3000	1360	10.5
Kibblewhite	Stratovolcano	34°34.576′ S	179°15.727′ E	13	1000	2000	1000	47.8
KI1	Satellite cone	34°29.308′ S	179°14.182′ E	6	1060	2000	940	7.2
KI2	Satellite cone	34°27.651′ S	179°14.071′ E	3.5	1380	2250	870	2.3
KI3	Satellite cone	34°34.571′ S	179°20.694′ E	5	1800	~2500	700	4.8
KI4	Satellite cone	34°41.058′ S	179°18.116′ E	6	1550	2500	950	8.9
Yokosuka	Stratovolcano	34°42.544′ S	178°32.717′ E	12	1060	2500	1440	52.4
Rapuhia	Stratovolcano	34°46.571′ S	178°30.319′ E	8	650	2250	1600	48.6
Giljanes	Stratovolcano	34°46.491′ S	178°34.723′ E	7	700	1800	900	39.9
Brothers	Silicic caldera	34°52.491′ S	179°04.523′ E	13–14	1350	2300	950	34.5
Healy	Silicic caldera	35°00.221′ S	178°58.357′ E	13–18	1100	2200	1100	68.9
Cotton	Satellite cone	35°02.691′ S	178°58.509′ E	4.8	980	1500	520	11.7
C2	Satellite cone	35°05.000′ S	178°57.700′ E	2.5	1600	2000	400	1.4
Silent II	Stratovolcano	35°10.118′ S	178°54.128′ E	14–17	780	2200	1420	86.8
Silent II (W)	Stratovolcano	35°12.600′ S	178°58.700′ E	9	1250	2100	850	15.4
Thompson	Stratovolcano	35°17.100′ S	178°51.750′ E	8–9	1250	2250	1000	14.9
Rumble II (W)	Stratovolcano/ summit caldera	35°21.200′ S	178°31.600′ E	17–22	1200	3000	1800	150.2
Rumble II (E)	Stratovolcano	35°25.100′ S	178°39.100′ E	12–17	1150	300	1850	78.9
Rumble III	Stratovolcano	35°44.377′ S	178°29.839′ E	22–26	220	3000	2780	261.9
Lillie	Satellite cone	35°51.217′ S	178°26.214′ E	9–11	1280	2120	840	42.0
Rumble IV	Stratovolcano	36°04.750′ S	178°00.750′ E	18–20	500	2550	2050	100.4
Rumble V	Stratovolcano	36°08.500′ S	178°11.750′ E	19–23	550	2600	2050	97.1
Tangaroa	Stratovolcano	36°19.252′ S	178°01.704′ E	16–18	600	2500	1900	74.2
Clark	Stratovolcano	36°26.780′ S	177°50.335′ E	13–15	860	2500	1640	92.0
		36°27.117′ S	177°50.195′ E		860			

transition from effusive pillow lavas, massive and sheet flows, and pillow and talus breccias to fragmental and scoriaceous hyaloclastite–pyroclastic deposits within water-depths of ~500–700 m (Wright, 1996; Wright et al., 2002). Basalts and andesites containing 47–58 wt.% SiO_2 are generally porphyritic and vesicular (Smith and Brothers, 1988; Gamble et al., 1993a, 1995). Rhyodacitic eruptions from the Healy caldera are interpreted to have been pyroclastic within water-depths of 500–900 m (Wright et al., 2003). Present-day hydrothermal venting (de Ronde et al., 2001; Baker et al., 2003) and/or associated sulfide mineralisation (Wright et al., 1998; de Ronde et al., 2003) are recorded from seven of the 13 volcanoes.

3. Data acquisition and analysis

Volcano mapping was undertaken using *RV Tangaroa*'s Simrad EM300 multibeam system that comprises 135 beams, with real-time beam steering compensating for ship motion. Motion sensing and positional navigation have accuracies of ≤0.02° and ± 5 m, respectively (Kleiner et al., 2001). Multibeam back-scatter and bathymetry data were edited and gridded at 25 m cell-size, with the latter having a vertical resolution of ~1–2 m within 2000 m water-depth. Seafloor photography from targeted 0.5- to 2-km-long tracks was completed at tow speeds of <1 knt. Similarly, rock sampling for each volcano was completed using both targeted and random dredging from 0.5- to 1-km long tracks. Edifice volumes were calculated from terrain models above curved basal surfaces defined for each volcano.

A total of 54 lavas were selected for whole-rock major element analysis. Despite the marine setting, very few glass crusts were recovered. Therefore, fresh cores were cut from lava blocks, coarse crushed, washed thoroughly in deionized water to remove possible sea-water salts, and then fine crushed in an agate mill. Dried powders were mixed with lithium tetraborate and ammonium nitrate, fused to a homogeneous glass bead, and analysed using the Philips 1400 XRF spectrometer at the University of Kiel calibrated against international rock standards. Loss on ignition was determined by weight loss of 3 g of powder heated to 1000 °C for 4 h in a silica crucible. Sample locations and a synoptic petrography are given in Appendix A.

4. Kermadec Arc (30°–35° S)

4.1. General

Twenty-two volcanoes with basal diameters >5 km are newly mapped (of which two are silicic calderas), with location, type of edifice, and synoptic physical dimensions given in Table 1 (including volcanoes

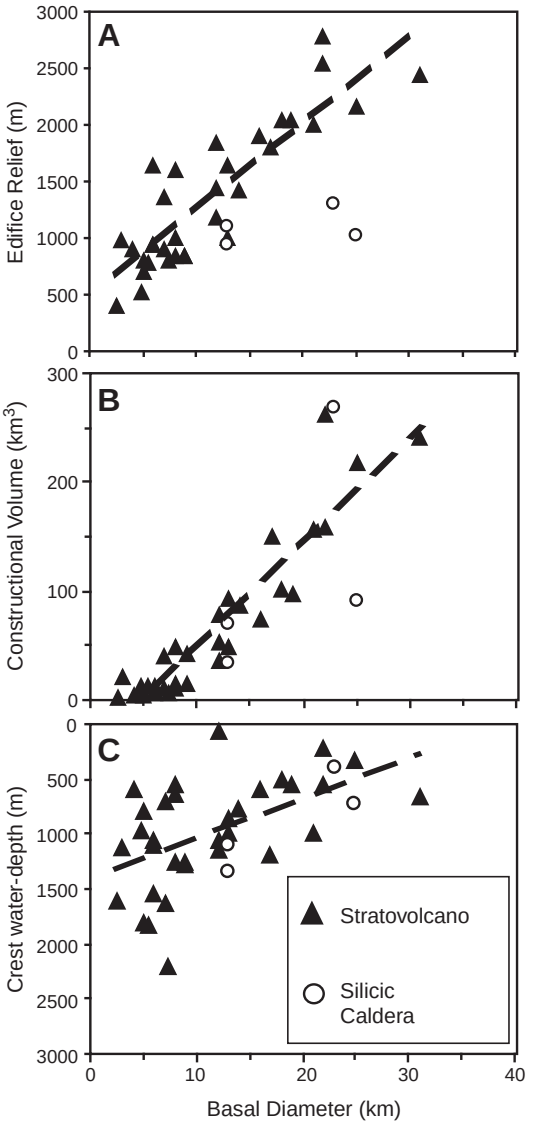

Fig. 3. Plots of edifice dimensions for Kermadec arc volcanoes at 30°–36°30′ S, showing generally consistent relationships of edifice relief and volume and crestal water-depth with volcano diameter.

south of 35° S). All volcanoes have consistent relationships of edifice relief, basal diameter, constructional volume, and summit water-depth (Fig. 3), though the silicic calderas have lower aspect ratios. The thirteen largest volcanoes are named and described here.

Following Lipman (1997), and previous Kermadec studies (Wright and Gamble, 1999), we use *caldera* (without reference to size or magma composition) for syn-eruptive collapse overlying a discharging magma chamber. *Crater* is used where volcanic ejecta form constructional collars surrounding the

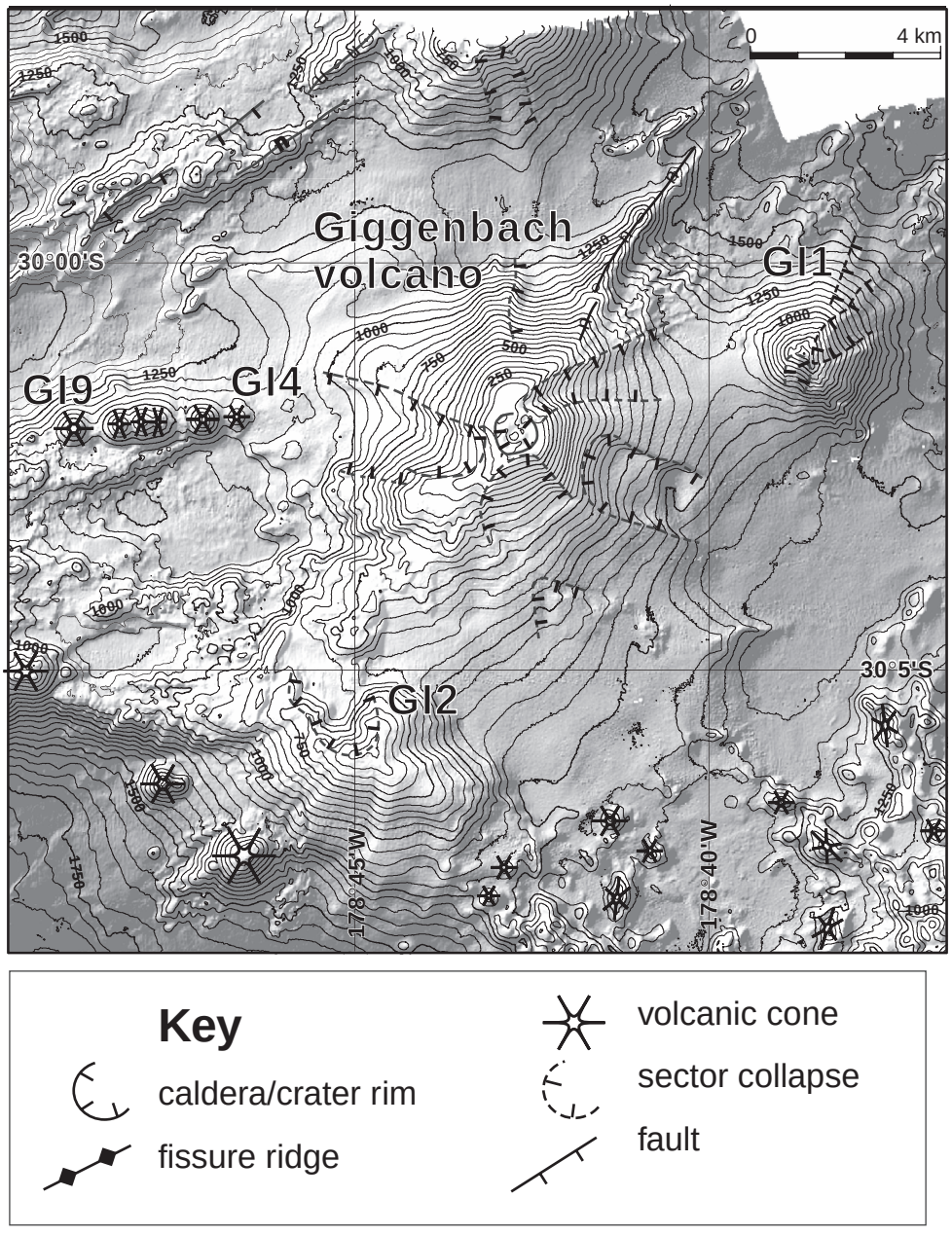

Fig. 4. Bathymetry and synoptic volcanic geology of Giggenbach volcano.

vent. In practice, the distinction can be difficult based solely on seafloor morphology (especially where the structure is overprinted or dismembered). However, where the structure is flat-floored we interpret it to be a caldera, and where the seafloor forms an inverted cone or paraboloid we interpret it as a crater.

4.2. Giggenbach volcano

Giggenbach volcano is elongate with an irregular morphology dominated by sector collapse (Fig. 4), and a prominent linear fissure dyke, orientated 037°, across the entire edifice. The edifice flanks comprise lavas (Fig. 5A) and volcaniclastic talus, with at least six separate phases of collapse/large-scale slumping. The flat summit, at a 120–100-m water-depth, is disrupted by a central, circular 700-m wide crater (partially breached to the north), in which a ~120-m wide cone shoals to 65 m. The youngest lavas from this cone, comprising aphyric dacite, are confined within the crater.

Satellite volcanoes occur east and south of Giggenbach volcano, with a further series of smaller aligned cones lying to the west. The eastern satellite volcano (GI1) is ~4.5 km in diameter and shoals to 600 m. Plagioclase basalt was recovered from the crest. Multiple sector collapses are observed on all flanks, with recent lava flows emitted only on the lowermost southeastern slope. The youngest collapse deposits from Giggenbach abut and post-date collapse deposits from GI1. The southern, ~8-km wide satellite cone (GI2) has a breached crater with large sector collapse on the northern flank, from which coherent blocks are distributed onto the lowermost southern flank of Giggenbach. Back-scatter imagery reveal recent lavas, emitted from southwestern flank fissures of GI2, has flowed around an older parasitic vent.

To the west of Giggenbach volcano, a 6–7-km wide zone of extensive and recent andesitic–dacitic

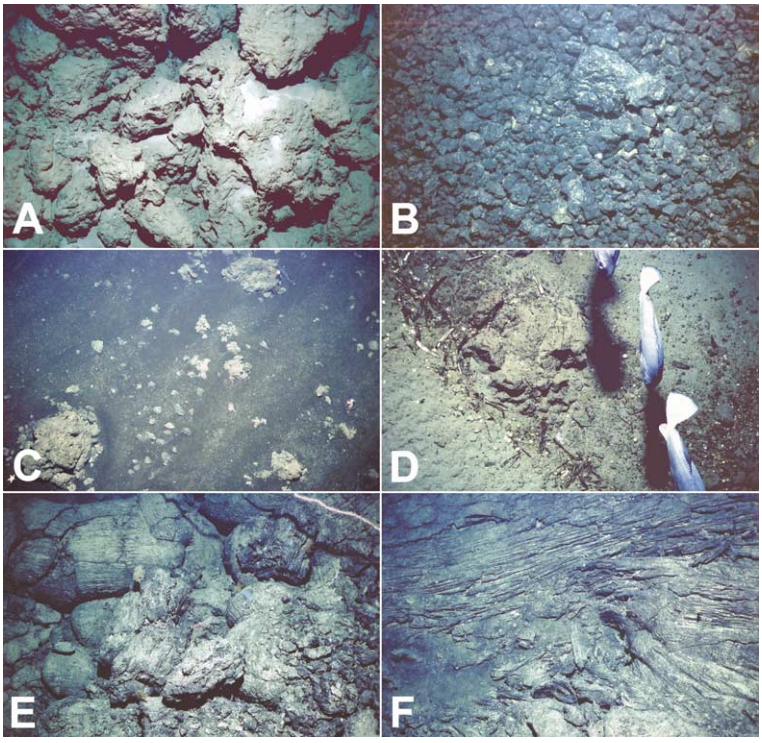

Fig. 5. Southern Kermadec volcano lava flows and volcaniclastic deposits. (A) Lavas on northwestern flank of Giggenbach volcano; TAN0205-69; (B) Volcaniclastic, including pumice clasts on lower Macauley caldera wall, TAN0205-61; (C) Lava breccia of Macauley cone, TAN0205-59; (D) Hydrothermal cone on Macauley caldera wall with *Bathyaustriella* vent biota, TAN0205-79. Freshly erupted pillow lavas (E) and sheet flows (F) on upper northeastern flanks of Haungaroa volcano, TAN0205-83. Field of view in all images is ~1–1.5 m.

lava flows (and extensional faulting) is bounded by eight vent cones (GI4–11) aligned east–west. Each cone is 0.7–1.5 km in diameter and 200–300 m high. The lower flanks of a further large edifice are imaged at the northern edge of the survey area.

4.3. Macauley volcano

Macauley volcano (Brothers and Martin, 1970; Lloyd et al., 1996; Smith et al., 2003a) is a large volcanic complex (at least 35 km in diameter) comprising (as exposed on Macauley Island) a sequence of basaltic shield lavas and phreatomagmatic deposits, the distinctive dacitic Sandy Bay Tephra Formation, and a cap of basaltic lavas. The Sandy Bay Tephra, sourced from the now submerged Macauley caldera (Figs. 6 and 7A), is dated at 6310 ± 190 ^{14}C yr (Lloyd et al., 1996). Multibeam data (though mostly of the western submarine flanks) shows the island represents <5% of the otherwise submerged volcanic complex.

The Macauley caldera, elongate along a strike of ~055°, is ~10.8 km long and ~8.2 km wide. The general structure of the caldera is a funnel, though both an inner linear fault (parallel to regional tectonic fabric) and an outer topographic rim form the south-eastern margin of the caldera. Pumice pervasively covers the caldera floor and lower wall (Fig. 5B). The topographic rim is generally between 500 and

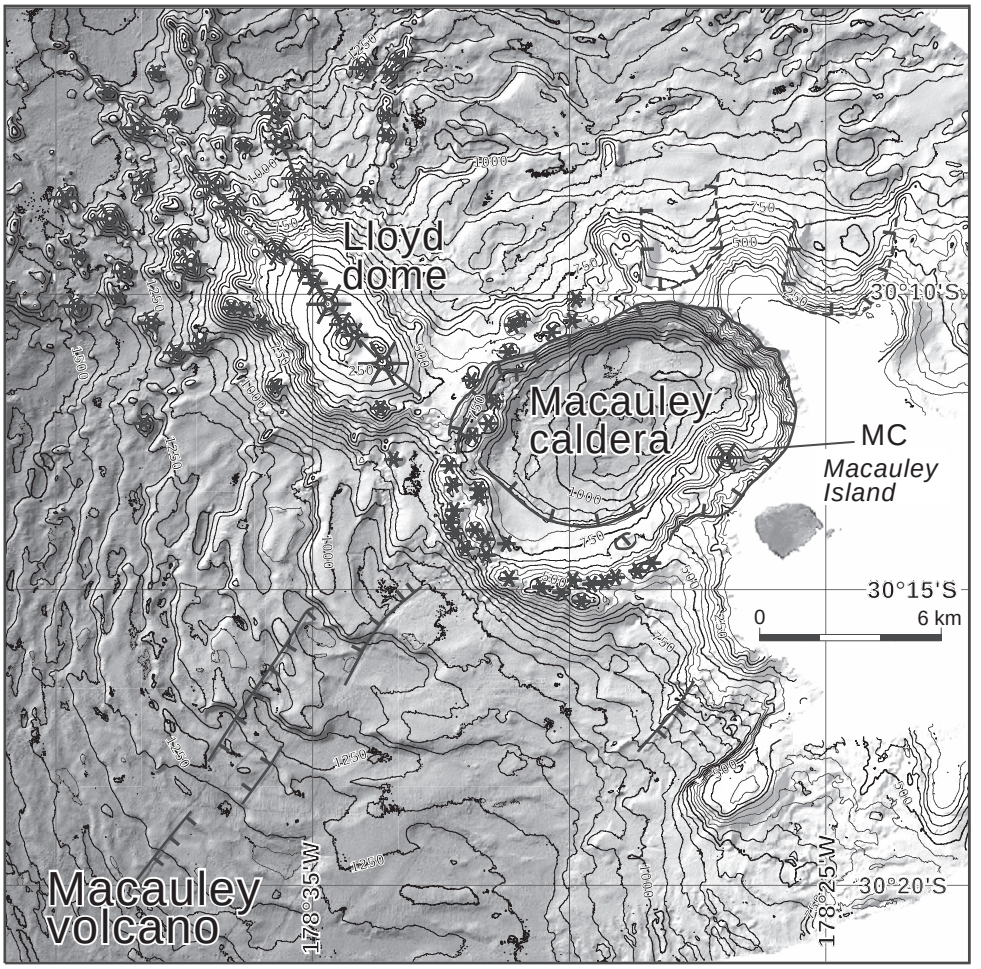

Fig. 6. Bathymetry and synoptic volcanic geology of Macauley complex including Macauley cone (MC) and caldera, and Lloyd dome. Interpretative key is given in Fig. 4.

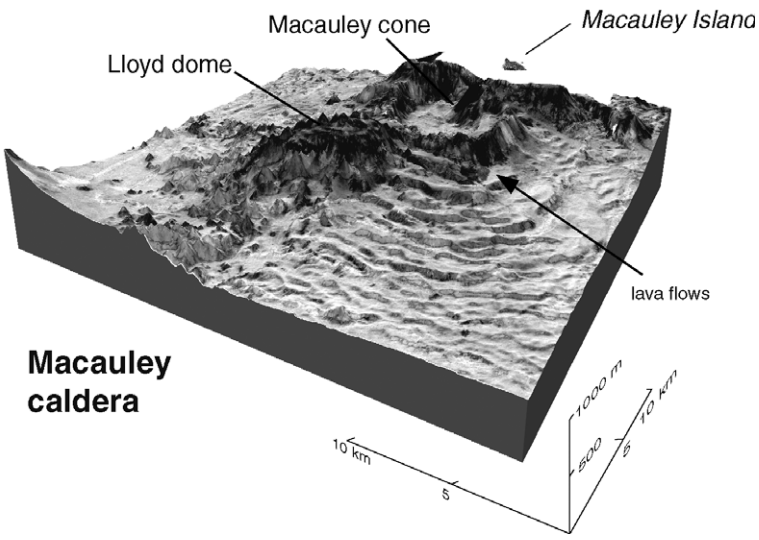

Fig. 7. EM300 back-scatter imagery draped over bathymetry terrain grids (cell size 25 m) for Macauley caldera volcano and associated Lloyd dome. Areas of high acoustic reflectivity (back-scatter) are shown as black/dark grey and are interpreted as recent lava flows, whereas areas of light grey are interpreted as sediment.

600 m in water-depth, but deepens to a rim depth of 750 m in the southeast, and conversely shallows to <100 m as the eastern wall ascends to the shoreline of Macauley Island. The topographic rim is capped by >30 vent cones along the western and southern rims that emit lavas both into the caldera and down the outer rim flanks. Sampled lavas from northern and southeast rim vents comprise aphyric and weakly porphyritic plagioclase dacite. A 700-m wide and 300-m high post-caldera cone coalesces with the inner eastern caldera wall, sited within 1.5 km of the island shoreline. The cone is young (as shown from back-scatter imagery, Fig 7A), and comprises aphyric dacite (Fig. 5C). It is an active hydrothermal site with a vent biota (Fig 5D). Partial collapse of the western caldera wall post-dates rim cone volcanism.

The western flanks of the complex mostly comprise a series of concentric ridges with relief of 100–110 m proximal to the crater rim, which progressively decrease in height to <10 m at distances of ~20 km. Seismic reflection data show these ridges as acoustically transparent units, interpreted as the correlative of the Sandy Bay Tephra, that thins laterally away from the caldera. The ridges have an internal hummocky structure, with minor vertical displacement, and are interpreted as mega bed-forms associated with eruptive Sandy Bay density flows and some penecontemporaneous edifice foundering. Onshore at least thirty individual Sandy Bay density flows are recognized (Lloyd et al., 1996).

To the northwest lies the elongate ~9 km long and 6 km wide Lloyd dome (Figs. 6 and 7A). The dome, with its crest at 300–500 m water-depth, is capped with a lineament of small cones that locally shoal to ~80 m water-depth. Basalt has been recovered from both the dome crest and capping cones, and dredged samples also included scoriaceous blocks, bedded fine-coarse ash blocks, finely laminated fine ash, bedded lapilli, and weathered pumice. A splay of small radiating vent cones forms the northwestern end of the dome.

4.4. Havre volcano

Havre volcano, ~25 km northwest of Havre Rock and L'Esperance, is a silicic caldera capping a 1-km high edifice (Fig. 8). The volcano flanks comprise a series of concentric escarpments and terraces, with small vent cones and fissure ridges emitting young lava flows. The concentric escarpments typically have relief of 100–150 m and, by analogy to the Macauley volcano, are interpreted as recording pyroclastic density flow mega-bedforms and syn-eruptive edifice foundering. Fissure ridges are orientated either

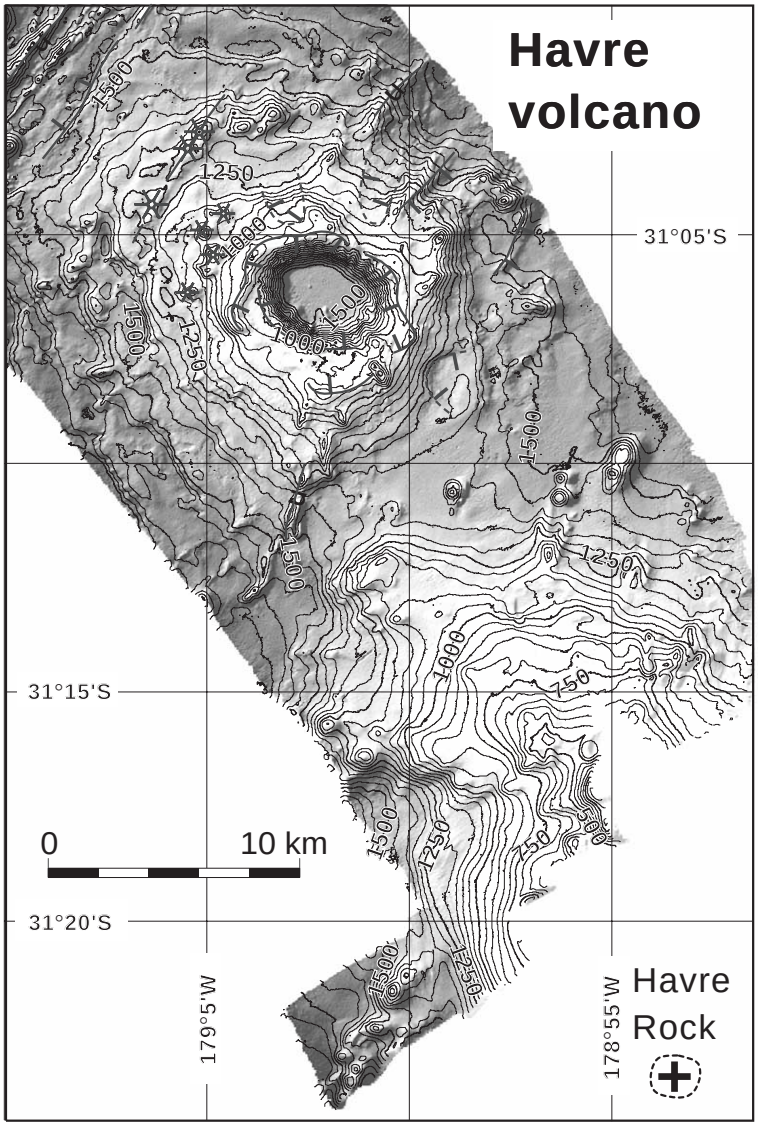

Fig. 8. Bathymetry and synoptic volcanic geology of Havre volcano. Interpretative key is given in Fig. 4.

radially or parallel with the back-arc rift fabric, and where combined form en echelon ridge structures.

The outer volcano flanks are predominantly mantled by "weathered" pumice, but include a lesser proportion of aphyric to plagioclase-bearing dacite and basalt lavas that form presumed pre-caldera lava sequences. Sector collapse is observed on the mid-upper outer flanks. Back-arc rifting extends into and dissects the lowermost western flanks, and in part post-dates the concentric structures. The southeastern flanks of the volcano merge with the western flanks of Kermadec Ridge and the subaerial Havre and L'Esperance volcanic stacks, with the latter composed of basalt (Gamble et al., 1990; Turner et al., 1997).

The caldera has an asymmetric morphology with the northern rim comprising mostly a single inner topographic wall, though in part it is segmented with arcuate and overlapping rims capped with post-collapse vent cones. In contrast, the southern rim

comprises both an outer topographic rim and inner wall separated by a 1.1–1.4-km wide terrace. Smaller craters occur on this terrace. Post-collapse vent cones cap the outer rim and uppermost outer flanks, with the youngest lavas flowing predominantly on the outer flanks. The largest post-collapse cone has three ~100–200-m wide craters.

The inner wall descends over 540 m to a flat 2.4–3-km wide caldera floor at a water-depth of 1520 m. The caldera walls are extensively modified by slumps up to ~1 km wide, with the associated toe deposits distributed on the caldera floor. Elsewhere, an elongate 700-m long fissure cone, with recent flows, extends onto the caldera floor. Rocks from the caldera wall include aphyric and plagioclase-bearing basalt–andesite, aphyric and plagioclase- and pyroxene-bearing dacite, gabbro, diorite, and pumice, all of which (except the last) are interpreted as a pre-caldera, stacked lava succession with intrusives. On the northern caldera wall this flow succession includes locally chloritised, hematised, and silicified lavas indicating past hydrothermal activity. Back-scatter imagery and seafloor photography show the caldera floor to comprise fine-grained volcaniclastic sediment, but include small pebbles of deeply altered pumice and aphyric plagioclase-bearing andesite, with the latter interpreted as shed from the caldera wall.

4.5. Oliver and Speight volcanoes

Oliver and Speight are satellite volcanoes ~7.5 and 5 km in diameter and shallow to water-depths of 2200 and 1840 m (Fig. 9). Both volcanoes sit on a larger arc massif enclosed by the ~3100 m isobath. They are elongate (particularly Oliver), dissected by exten-

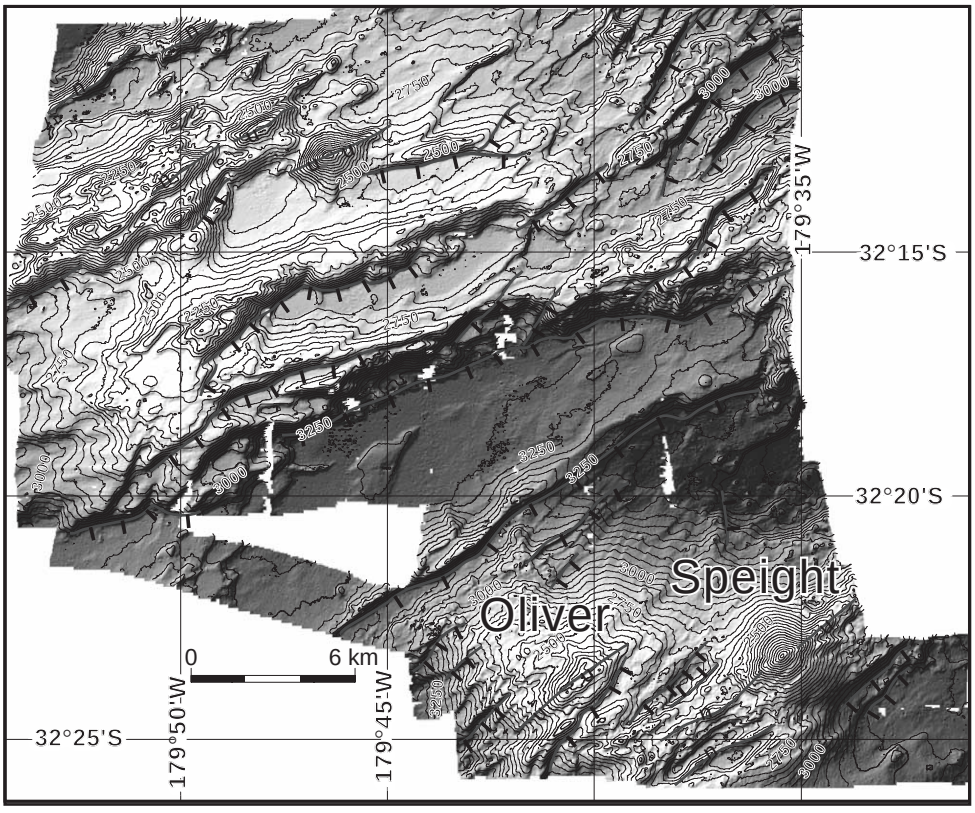

Fig. 9. Bathymetry and synoptic volcanic geology of Oliver and Speight volcanoes. Interpretative key is given in Fig. 4.

sional faults and 1–2-km long fissure ridges orientated 050°–055°, with the former bounding small pull-apart basins and flank rifts on the lower volcano flanks. High back-scatter from both cones is consistent with the recovery of fresh aphyric and plagioclase–pyroxene-bearing basaltic andesite. Immediately north of the arc massif, the back-arc region comprises extensional rift faulting and associated elongate fissure ridge volcanic cones, variably orientated between 015° and 073°.

4.6. Haungaroa volcano

Haungaroa volcano, with a summit crater, is a large stratovolcano rising over 2400 m in relief to a caldera rim water-depth of ~660 m (Fig. 10). The lower-mid flanks are a complex distribution of volcaniclastic talus (including pumiceous clasts), lava flows, and fissure ridges (Le Gonidec et al., 2003). The summit crater is elongate (trending 134°) and surrounded by a discontinuous and segmented 50–100-m high wall.

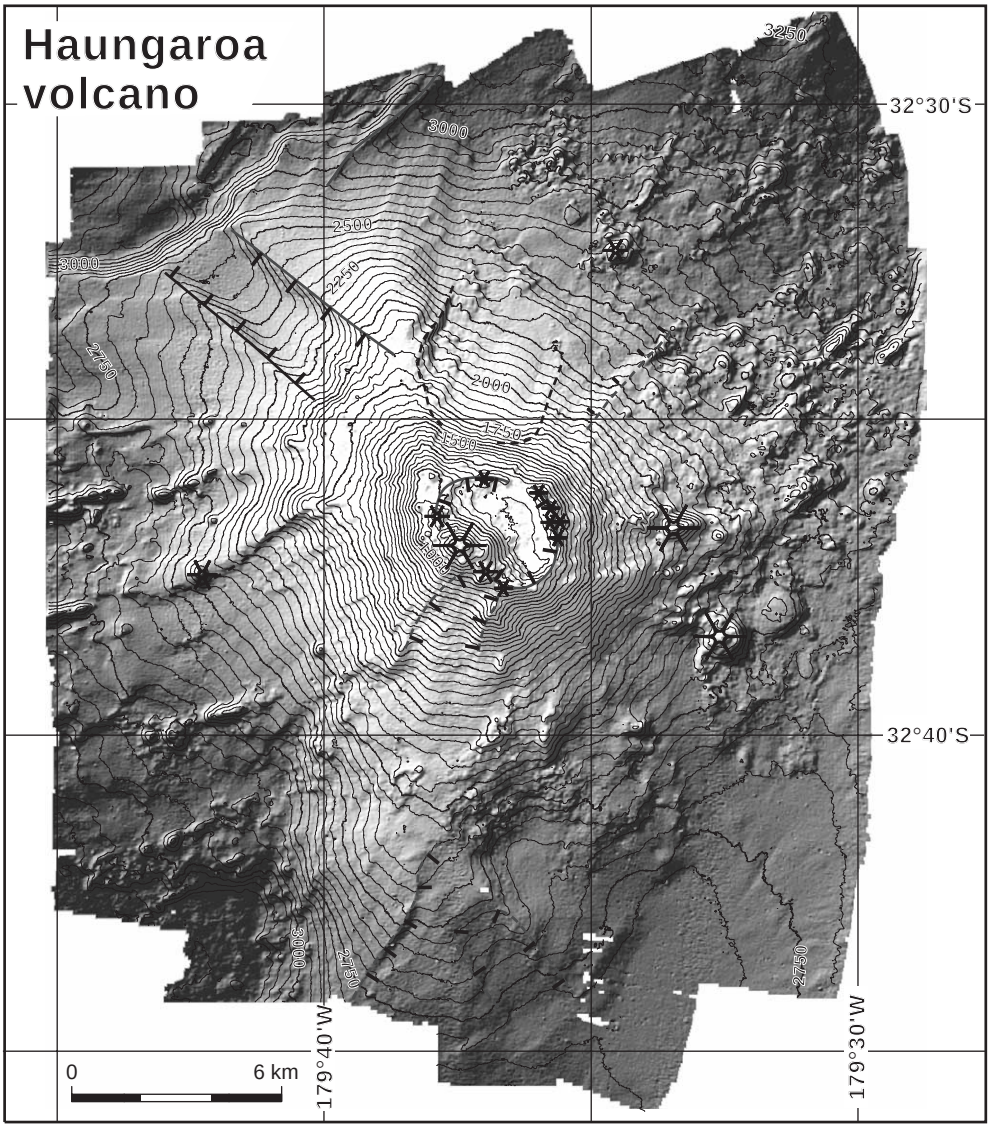

Fig. 10. Bathymetry and synoptic volcanic geology of Haungaroa volcano. Interpretative key is given in Fig. 4.

Aphyric basaltic andesite and weathered plagioclase–pyroxene basalt were recovered from the inner western wall. The crater rim is studded with younger cones with lavas flowing both into the crater and down the outer flanks. The largest, a 300-m high cone, coalesces with and buries the southwest wall, partially infilling the crater.

Extensive lava flows (Fig. 11) comprising aphyric and sparsely plagioclase phyric basaltic andesite, sourced from vents on both the crater rim and the northern flanks, have "resurfaced" ~30% of the edifice. These pristine flow fields include both pillow lavas and tubes (Fig. 5E), and localized sheet flows indicative of higher rates of magma discharge (Fig. 5F). The flow fields post-date a significant phase of sector collapse of the northern flank. Older, plagioclase pyroxene basalt and basaltic andesite from the northern flank, partially buried by the sparsely phyric basaltic andesite lavas, record an earlier phase of edifice construction.

Sector collapse is observed on much of the volcano, but is most pronounced on the western and southern flanks, where "resurfacing" by basaltic andesite flows is confined to the uppermost flanks. These latter flows are, in turn, disrupted by surficial sliding and slumping. Sector collapse has partially exposed radial fissure dike ridges on the lower southwest flanks. On the northwestern flank, a 2-km wide rift trending 132° extends to the edifice summit.

4.7. Kuiwai volcano

Kuiwai volcano is a semi-circular stratovolcano rising to a summit water-depth of 560 m, and includes the satellite KU1 cone on its western flanks (Fig. 12). The main edifice is surfaced with massive and bulbous lavas, lava breccias (Fig. 13A), and block to tuff-sized volcaniclastic sediments. The summit is interpreted to comprise two dismembered craters. The older, and only partially remnant, crater is ~700 m wide with 40–80 m high walls. The younger crater, overprinting much of the older vent, is 800–850 m in diameter with a breach on the northern rim. The latter forms the head of a large sector collapse on the northern flank. Over 20 small elongate and aligned vent cones stud the northern flanks. They, and associated fissure ridges, trend 033°–050°. Likewise, a ~3 km wide-curvilinear fissure ridge trends 033°, extending over 9 km from the lower northwest flank.

Significant sector collapse, observed on the both northern and southwestern edifice flanks, has partially

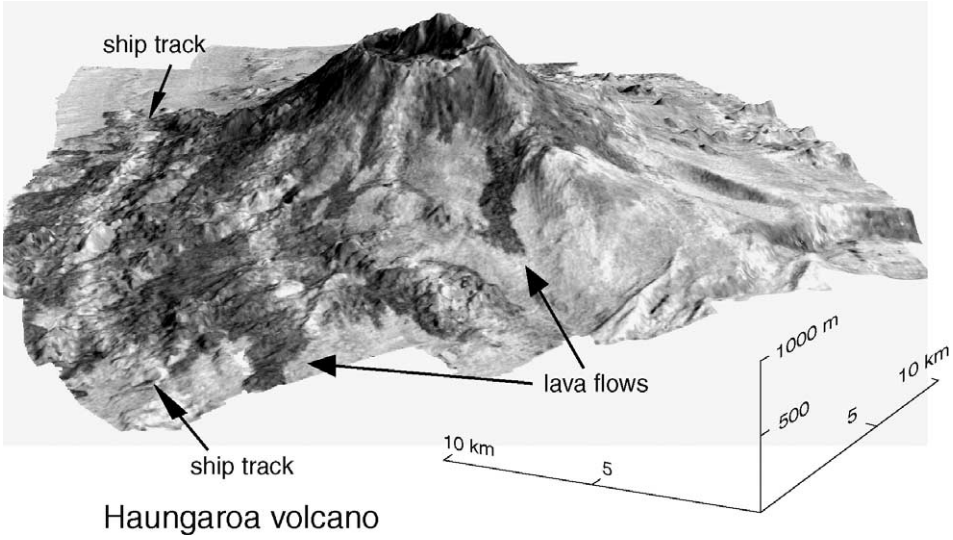

Fig. 11. EM300 back-scatter imagery draped over bathymetry terrain grids (cell size 25 m) for Haungaroa volcanoes. Areas of high acoustic reflectivity (back-scatter) are shown as black/dark grey and are interpreted as recent lava flows, whereas areas of light grey are interpreted as sediment.

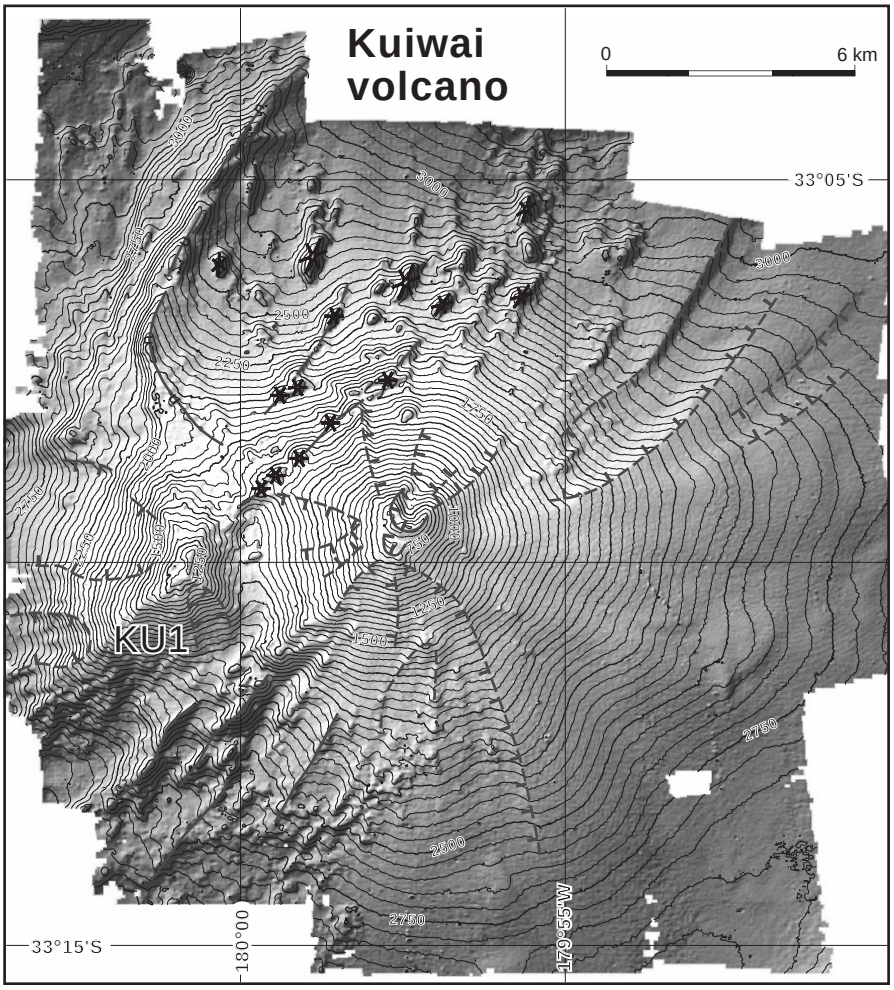

Fig. 12. Bathymetry and synoptic volcanic geology of Kuiwai volcano. Interpretative key is given in Fig. 4.

exposed radial and tectonic-aligned fissure feeder dikes. Localized sliding and slumping is also observed on the western flank, including a >8-km wide flank rift. Less prominent slumps, including toe deposits, are interpreted as older failures partially "fused" with subsequent volcaniclastic apron deposition.

The elongate satellite KU1 volcano, rising to 1120 m summit water-depth, post-dates much of the sector collapse and slumping of the main southern flank. The western flank of KU1, in turn, shows evidence of collapse and slumping over almost its full relief. Elongation of the KU1 edifice trends 045°, forming a prominent vent lineament with smaller cones of the main edifice.

Lavas from the main Kuiwai summit comprise moderately "weathered" plagioclase basaltic andesite, with more "weathered" plagioclase basalts recovered from the edifice flanks. In addition, gabbros were recovered from a sector collapse headscarp on the southwest flank. Consistent with high back-scatter imagery, is fresh plagioclase pyroxene basalt from the KU1 cone.

4.8. Ngatoroirangi volcano

Ngatoroirangi volcano is a semi-circular stratovolcano rising to crestal water-depth of 340 m (Fig. 14). The edifice flanks comprise volcaniclastic deposits

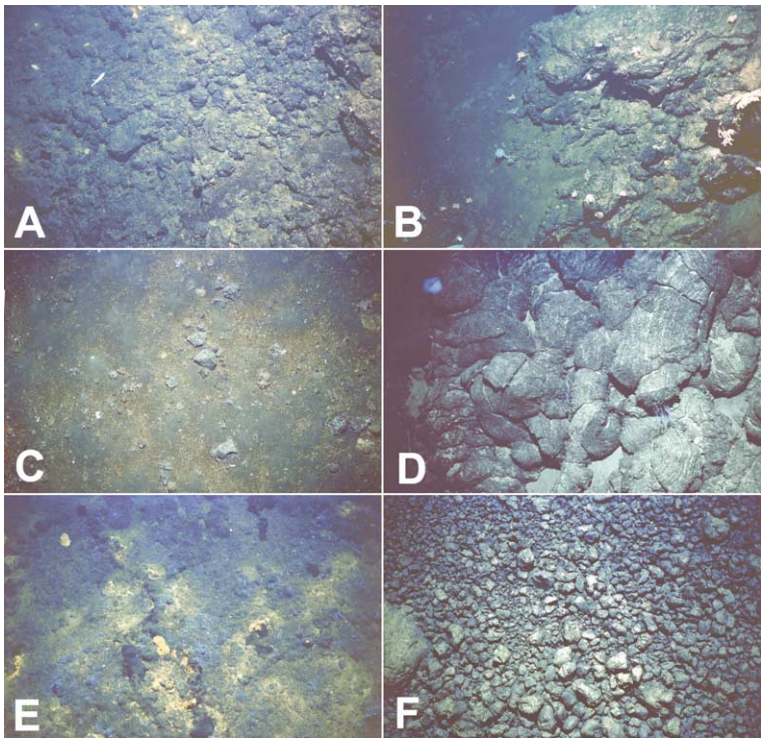

Fig. 13. Southern Kermadec volcano lava flows and volcaniclastic deposits. (A) Massive lavas on crater rim of Kuiwai volcano, TAN0205-84; Massive lavas (B) and volcaniclastic deposits (C) on upper northwest flank of Ngatoroirangi volcano, TAN0205-87; (D) Freshly erupted pillow lavas from satellite SO1 volcano, TAN0205-93; ?Hydrothermally altered lavas and coarse volcaniclastic deposits (E) and lava breccias (F) on upper southern flank of Kibblewhite, TAN0205-103. Field of view in all images is ~1–1.5 m.

and lava flows dissected by various sector collapses. Volcaniclastic deposits are dominantly granule lapilli-sized clasts, but include coarser blocks and breccias (Fig. 13B and C). Back-scatter imagery reveals both volcaniclastic deposits and lavas form radial and distributary aprons and flows sourced mostly from the summit. Individual flows are massive and lack obvious flow fabric. Sampled lavas from the summit crater are both fresh and hydrothermally altered plagioclase phyric basalt and basaltic andesite. Strongly plagioclase phyric basalt and basaltic andesite also occur on the northeastern and southwest flanks. More recent flows extend >4–5 km down the northern and southeast flanks.

At least five separate sector collapses, some with multiple phases of slumping, occur along the western and southern flanks of the edifice. In most cases the collapse extends over the full relief of the edifice, with the headscarp extending to the uppermost flanks and crest, though individual slide volumes are typically <1 km^3. Most slumping on the southern and northeastern flanks is aligned and/or controlled by faults striking 042°–048°.

4.9. Sonne volcano

Sonne (Haase et al., 2002) is a large stratovolcano with summit calderas and a series of four prominent radiating ridges, including the connection to the satellite SO1 volcano (Fig. 15). The edifice flanks comprise effusive lavas and associated coarse breccias, plus extensive deposits of granule-sand sized volcaniclastic sediments. Lavas from the mid-upper flanks are heterogeneous, and include plagioclase basaltic andesite, aphyric andesite and dacite, pumice, and olivine plagioclase basalt, together with diorite on the NE mid-flank. Extensional faulting, especially in the southeast (striking typically 035–045 °), and sec-

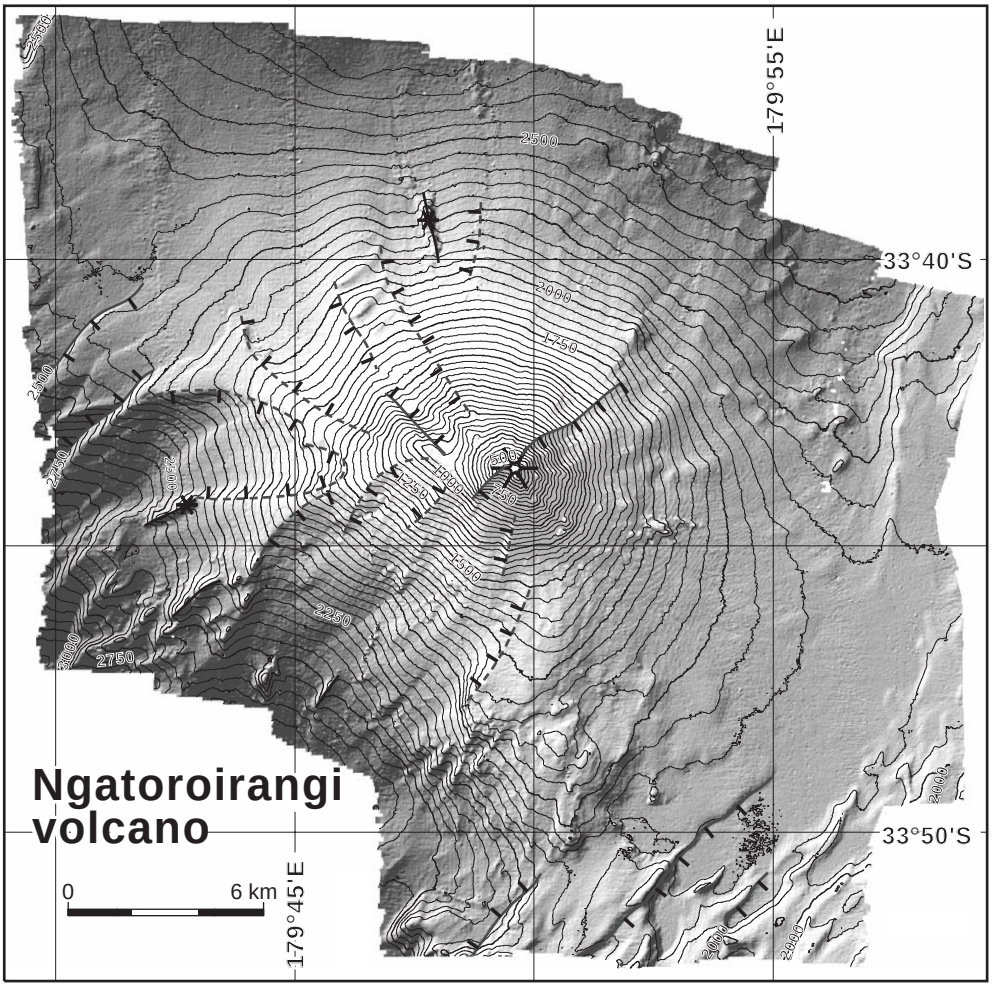

Fig. 14. Bathymetry and synoptic volcanic geology of Ngatoroirangi volcano. Interpretative key is given in Fig. 4.

tor collapse extensively dissect the radiating ridges and upper volcano flanks. At least 10 separate sector collapses are identified, principally along the southern flank. A further volcano (only partially mapped), rising at least 600 m in relief and coalescing with the lowermost northwest flank, is similarly dissected by rift faults.

At the summit, three nested calderas are identified (Fig. 15). The outer (and oldest) and intermediate calderas have diameters of 2.3–2.6 and 1.6–2 km, respectively, with walls coalescing in the north and rising to a maximum 100–120 m above the 1120-m deep crater floor. A 500–600-m wide cone coalesces with the southern intermediate caldera wall. Sector collapse has removed part of the outer caldera rim, which we interpret to pre-date formation of the intermediate caldera since the corresponding section of the latter rim is intact. The innermost crater is 0.8–1 km wide, has a 60–100-m high wall, and a central 100–130-m wide cone. Fresh aphyric and plagioclase-bearing dacite, including some pumiceous forms and more "weathered" equivalents, were recovered from the summit. Back-scatter imagery reveals recent eruptions from the inner crater which are distributed to both the intermediate caldera and uppermost slopes of the eastern sector collapse. A breached caldera is also sited on the mid-upper northwestern flank at the margins of another large sector collapse, though any temporal link between caldera eruption and sector collapse is presently speculative. That caldera has a topographic

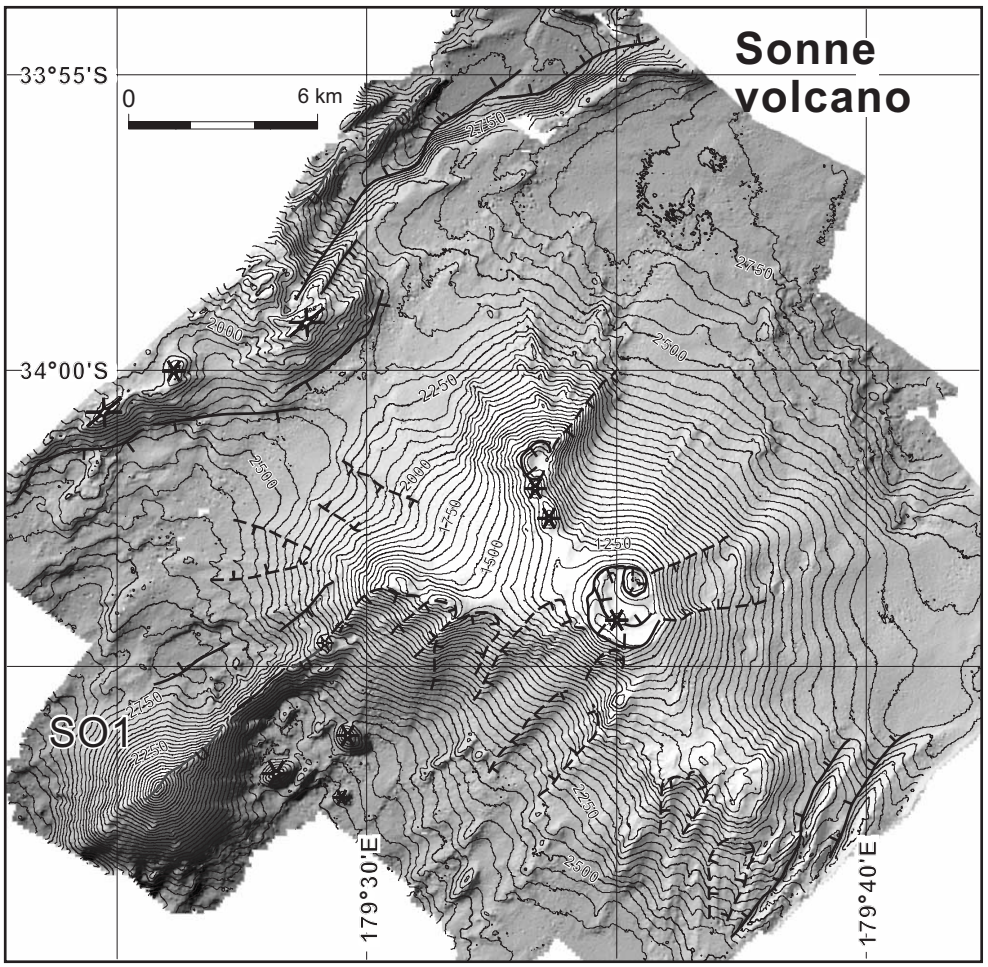

Fig. 15. Bathymetry and synoptic volcanic geology of Sonne volcano. Interpretative key is given in Fig. 4.

width of ~850–900 m, with the 120-m high walls rising to a water-depth of 1200–1240 m at the rim. Other small dismembered calderas are interpreted on the upper southern flanks within water-depths of ~1400 m.

On the lower southwest flank, the elongate satellite SO1 volcano is linked to the main edifice via a 2-km long, 300-m high, linear fissure ridge (orientated 048°) that narrows to ~160 m width at its crest. SO1 lavas (Fig. 13D) are plagioclase–pyroxene basalt and basaltic andesite, and the back-scatter imagery suggests they are younger than most Sonne flank lavas. Deeply weathered pyroxene basalt was recovered from the saddle of the ridge linking Sonne with the SO1 volcano.

4.10. Kibblewhite volcano

Kibblewhite volcano (Fig. 16) is a composite edifice rising to a summit at 1000 m water-depth, and is surrounded by a cluster of four satellite cones. The main cone is elongate (trending 138°), linking two fissure ridges that protrude northeast and southwest for ~9 km along broad trends at 045°. In detail though, both ridges have sigmoidal configurations. At the crest, three <500-m wide, partially coalesced, craters are aligned and controlled by a tectonic lineament parallel to the edifice elongation. On the southern flank, sector collapse headscarps have partially destroyed two of the summit craters. Dacite with devitrification banding, basaltic andesite pillow

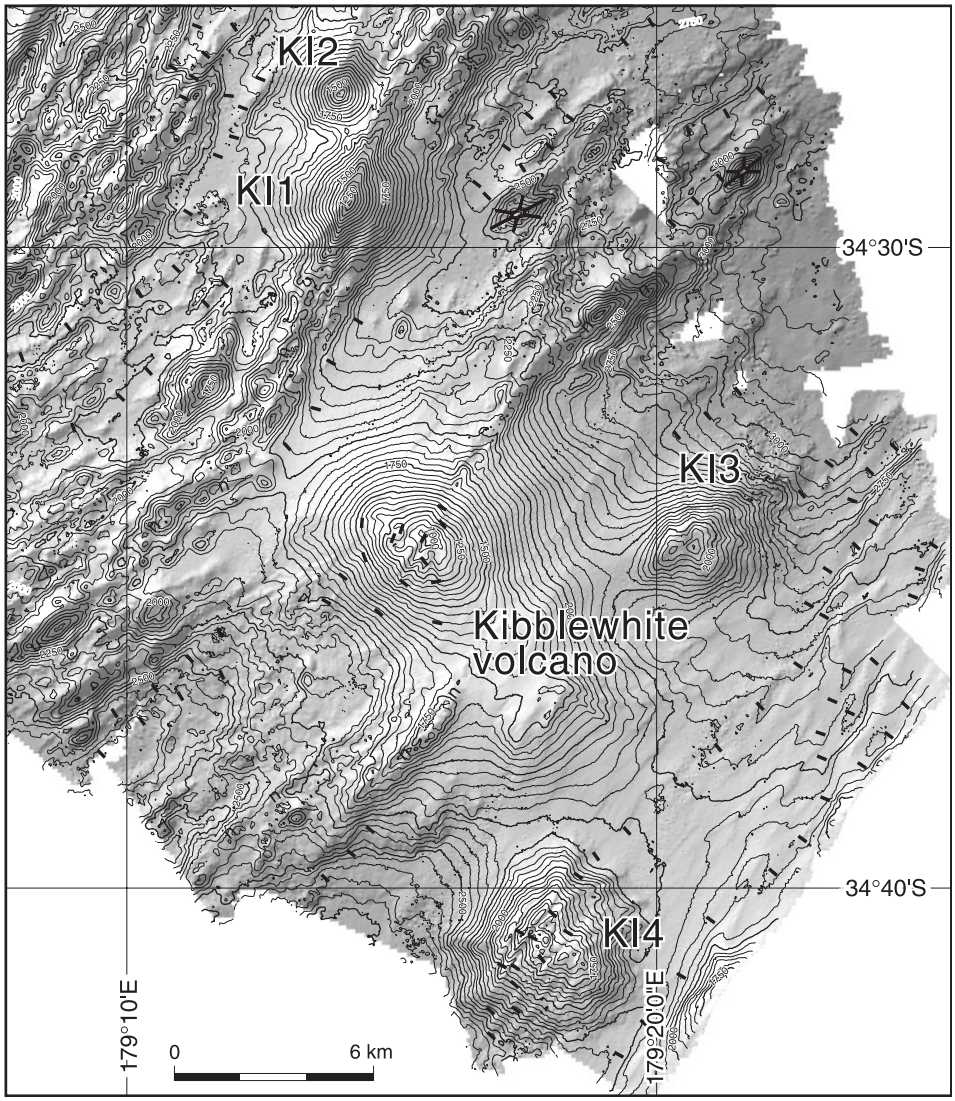

Fig. 16. Bathymetry and synoptic volcanic geology of Kibblewhite volcano and satellite cones. Interpretative key is given in Fig. 4.

lavas, hydrothermal alteration (Fig. 13E), and lava breccias (Fig. 13F) are recorded from the volcano crest and upper flanks.

To the north, the satellite KI1 and KI2 cones are younger vents. The KI1 edifice is strongly elongate, with fissure ridges extending both northeast and southwest in a sigmoidal arrangement. Plagioclase basalt was recovered from the KI1 cone. Further west, a pervasive sigmoidal fabric of extensional faulting, elongate vent cones, and fissure ridges extends over at least 30 km. In the east, the KI3 satellite cone on the main edifice mid-flanks is similarly elongate, with minor sector collapse on its northwest flank. Pumice has been recovered from the crest. In the south the KI4 satellite cone rises to ~1550 m water-depth and includes a ~500-m wide crater at its crest. The edifice lies <10 km from the frontal Kermadec Ridge, and is extensively dissected by normal faults. Weathered olivine–pyroxene basalt was recovered from the cone crest.

4.11. Rapuhia, Yokosuka, and Giljanes volcanoes

Rapuhia, Yokosuka, and Giljanes volcanoes (Fig. 17) form a cluster of composite cones atop an elevated, but pervasively rifted massif block, ~45 km behind the active arc front. Yokosuka, shoals to 1060 m water-depth and is a degraded cone with an array of vent alignments and extensive sector collapse. Individual vent cones are typically <500 m wide and 200 m high. On its northwestern flank, the largest sector collapse extends over almost the full relief of the edifice, with the associated debris avalanche extending to water-depths of ~2800 m. Post-collapse cones (the largest being ~2 km wide and 300 m high) are aligned 125°, and have formed both within the collapse amphitheatre and through and atop the debris avalanche deposit. Strongly weathered dacite, plagioclase andesite, and pumice were recorded from the cone summit.

To the southwest, Rapuhia stratovolcano is a younger and largely pristine edifice rising to a 650-m summit water-depth. It is elongate along a trend of 065°, defined in part by a prominent fissure ridge and vent alignment to the southwest and northeast, respectively (Fig. 17). Back-scatter imagery show the former is the site of extensive and recent volcanism. Minor surficial slumping scars the northern flanks. Weathered basaltic andesite and dacite were recovered from the main edifice crest, but presumably do not represent the most recent volcanism. Lying due east, Gil-

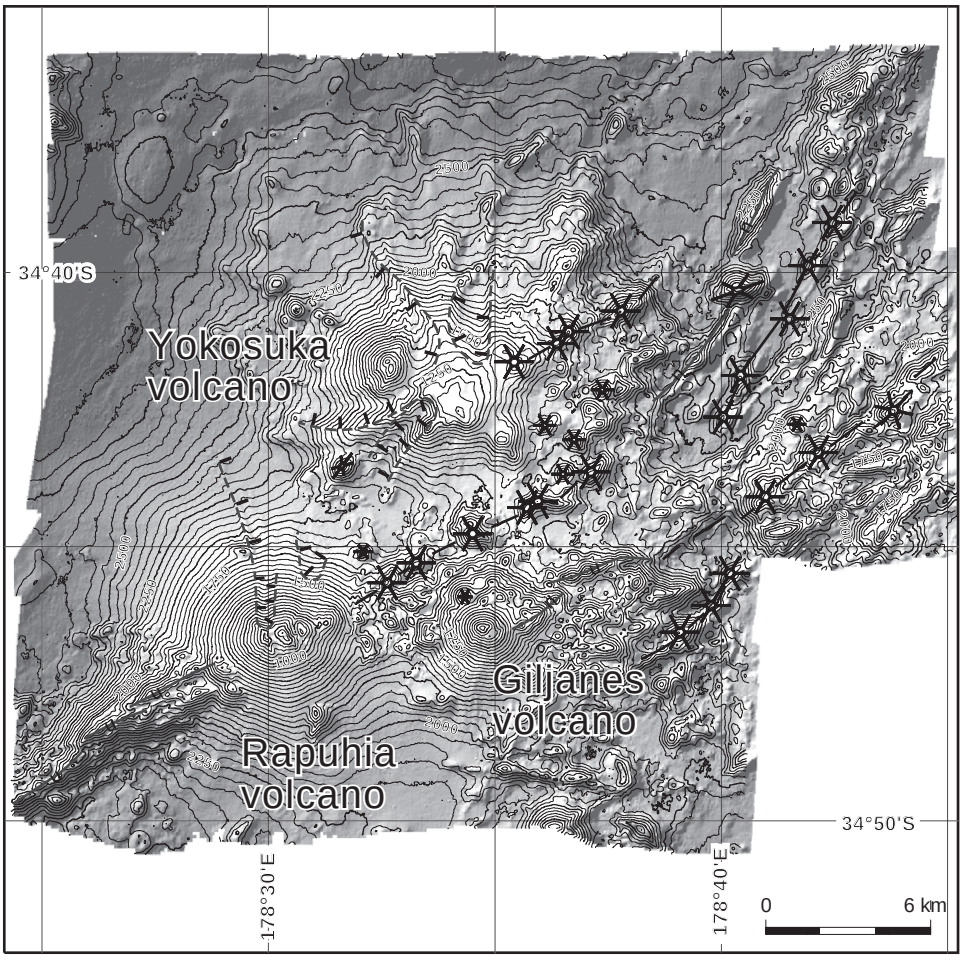

Fig. 17. Bathymetry and synoptic volcanic geology of Yokosuka, Rapuhia, and Giljanes volcanoes. Interpretative key is given in Fig. 4.

janes volcano is a smaller equant, cone, rising to a 700-m summit water-depth. Weathered plagioclase pyroxene andesite and a block of bedded manganese oxides, inferred to represent a hydrothermal deposit, were recovered from the crest. Small fissure ridges protrude from the lower northeast flank, extending to a more pervasive region of fissure ridges, elongate cones, vent alignments, and rift tectonics.

5. Major element geochemistry

Fifty-four whole-rock major element analyses from the 30° to 35° S sector of the Kermadec arc are given in Table 2. Lavas erupted by the 30°–35° S volcanoes form a distinctly bimodal distribution dominated by basalt–basaltic andesite (typically 48–55 wt.% SiO_2) with subordinate dacite, consistent with previous observations concerning Kermadec arc volcanism (Fig. 18A). Dacite accounts for ~31% of the analysed lavas, whereas less than 7% of the lavas have intermediate compositions. Caldera complexes such as Macauley and Havre (and Brothers and Healy further to the south) are dominated by silicic lavas that extend from the dacite field to transitional rhyolite with ~72 wt.% SiO_2, although lesser outcrops of basalt and basaltic andesite may pre-date (Macauley, Havre) or post-date (Healy) the youngest caldera-forming event. Dacite, though, is not restricted to the caldera complexes and lavas with >66 wt.% SiO_2 were recovered from the Sonne, Giggenbach, and Rapuhia stratovolcanoes (Table 2). Nevertheless, dacite has not yet been recovered from the largest stratovolcanoes dredged during this study (Ngatoroirangi, Kuiwai, Haungaroa).

Most Kermadec arc lavas can be classified as members of the low-K series from a K_2O vs. SiO_2 plot, although some are transitional to the medium-K series and a few are significantly enriched in K_2O (Fig. 18B). Mafic lavas from individual volcanoes on the arc front form sub-parallel arrays on a K_2O vs. SiO_2 plot, with closely overlapping arrays at the lowest K_2O for Ngatoroirangi, Kuiwai, Haungaroa, Speight and Raoul. Distinctly higher in K_2O, but still within the low-K series, are lavas from Kibblewhite, Havre and Macauley. Lavas from Giggenbach, Giljanes, Rapuhia and Yokosuka form arrays plotting within the medium-K series field, and it is notable that these four stratovolcanoes are situated significantly west of the arc front (up to 45 km). However, the few high-K series lavas outcrop together with low-K series lavas on stratovolcanoes at the arc front (SO1 volcano—this study; Clark—Gamble et al., 1997). Greater intervolcano differences are shown by the silicic lavas from the caldera complexes. Healy, Havre, and Macauley dacite have higher K_2O than Raoul dacite, but all plot within the low-K series field. In contrast, Brothers dacite plots within the medium-K series field.

Considerable scatter about general trends on major element variation diagrams reflects the strongly porphyritic character of mafic and intermediate Kermadec lavas (Fig. 19). Although Mg-numbers (Mg#) range from 23 to 79, lavas with Mg# >60 contain >20% clinopyroxene phenocrysts together with >5% olivine phenocrysts. Ubiquitous plagioclase phenocrysts range from trace quantities to >30% of the mode, and impart much scatter to plots featuring CaO and Al_2O_3. Nevertheless, an inflection in TiO_2 vs. Mg# is attributed to the onset of Ti-magnetite fractionation at Mg# ~40.

6. Discussion

6.1. Kermadec silicic volcanism

Silicic volcanism, including caldera-forming eruptions, is increasingly recognized as a significant and important aspect of both the Kermadec arc (Worthington et al., 1999; Wright and Gamble, 1999; Smith et al., 2003a,b), and intra-oceanic arc magmatism in general (e.g., Tamura and Tatsumi, 2002; Leat et al., 2003). A compilation of 199 whole-rock analyses from 22 Quaternary edifices along the Kermadec arc between 30° and 36°30′ S, including those presented here, confirms the basic bimodal basalt–basaltic andesite vs. dacite character of Kermadec magmatism (Fig. 20A). Recognizing the caveats of under-sampling and limitations of surficial rock-dredging, we take this further by calculating volume-weighted histograms for each lava type using the method of Aramaki and Ui (1978) and the edifice volumes presented in Table 1 (Fig. 20B and C). These volume-weighted histograms yield remarkably similar relative proportions and total volumes for each lava type compared to

Table 2
Whole-rock major element geochemistry of arc volcanoes from the 30°–35° S sector of the Kermadec arc

Volcano	Giggenbach						Macauley					Havre		
Lat.	30°02.2′ S	30°02.7′ S	30°02.5′ S	30°02.1′ S	30°02.1′ S	30°01.1′ S	30°12.8′ S	30°09.9′ S	30°14.6′ S	30°10.8′ S	30°10.0′ S	31°04.8′ S	31°05.1′ S	31°05.1′ S
Long.	178°42.9′ W	178°42.1′ W	178°50.5′ W	178°48.3′ W	178°43.0′ W	178°38.8′ W	178°27.0′ W	179°29.9′ W	178°33.3′ W	178°34.4′ W	178°34.5′ W	179°01.5′ W	179°03.4′ W	179°03.4′ W
Depth (mbsl)	143	605	1061	979	153	783	492	694	1038	123	308	1027	941	941
Sample	65-01	67-04	72-01	73-01	74-01	77-02	55-01	60-01	62-01	63-01	64-01	45-02	46-01	46-03
SiO_2	65.82	50.96	65.80	60.50	64.74	47.51	66.83	63.03	63.64	45.37	48.06	70.33	69.84	51.88
TiO_2	0.67	0.93	0.61	0.82	0.60	0.94	0.82	0.86	0.93	0.80	0.85	0.54	0.40	1.31
Al_2O_3	15.14	16.61	14.85	16.15	15.29	17.93	13.52	14.02	12.99	17.25	17.20	13.72	13.95	14.89
Fe_2O_3	4.87	10.49	4.43	6.30	4.30	12.00	6.00	7.90	7.83	12.51	12.28	3.83	3.92	12.49
MnO	0.12	0.17	0.11	0.14	0.24	0.19	0.17	0.17	0.18	0.20	0.20	0.10	0.16	0.18
MgO	1.32	5.65	0.91	1.98	1.18	4.94	1.25	1.64	1.52	7.64	6.35	0.78	0.58	4.48
CaO	3.33	11.28	2.90	4.82	3.65	12.25	4.17	5.06	4.69	12.12	11.88	2.77	2.86	8.95
Na_2O	4.71	2.57	4.71	4.40	4.67	2.00	4.26	4.35	4.10	1.82	1.99	4.92	4.83	3.03
K_2O	2.75	0.72	2.98	2.38	2.52	0.89	1.37	1.09	1.18	0.32	0.52	1.51	1.42	1.04
P_2O_5	0.19	0.14	0.18	0.37	0.18	0.23	0.27	0.25	0.30	0.12	0.14	0.11	0.11	0.25
LOI	0.29	−0.16	1.03	0.86	1.78	−0.24	0.57	0.59	1.44	1.12	0.10	0.11	1.36	1.20
Total	99.21	99.35	98.51	98.72	99.15	98.64	99.21	98.96	98.80	99.27	99.57	98.61	99.40	98.50
Mg#	35.8	52.6	29.7	39.3	36.1	45.9	29.9	30.0	28.6	55.7	51.6	29.6	23.2	42.5

Volcano	Havre			Oliver		Haungaroa						Kuiwai		
Lat.	31°08.0′ S	31°05.9′ S	31°08.4′ S	32°23.5′ S	32°23.5′ S	32°36.9′ S	32°35.8′ S	32°35.8′ S	32°38.5′ S	32°32.9′ S	32°32.9′ S	33°09.4′ S	33°09.4′ S	33°09.9′ S
Long.	179°00.8′ W	179°06.1′ W	179°00.5′ W	179°40.2′ W	179°40.2′ W	179°37.8′ W	179°38.3′ W	179°38.3′ W	179°34.2′ W	179°39.3′ W	179°39.3′ W	179°57.5′ W	179°57.5′ W	179°59.1′ E
Depth (mbsl)	809	1260	956	2340	2340	815	1167	1167	2186	2135	2135	640	640	1264
Sample	47-03	49-01	51-01	43-01	43-03	34-01	37-01	37-03	38-01	82-01	82-03	27-01	27-04	28-01
SiO_2	67.19	70.59	70.08	53.97	53.28	55.74	55.70	51.48	56.27	51.51	54.17	58.23	54.11	52.58
TiO_2	0.66	0.40	0.42	0.99	0.70	1.03	1.06	0.61	1.06	0.54	0.74	0.83	0.73	0.70
Al_2O_3	14.65	14.13	13.49	16.29	16.94	14.73	14.70	17.91	14.12	18.30	18.00	16.16	16.64	16.27
Fe_2O_3	4.51	3.87	2.86	9.11	8.81	11.70	11.55	9.71	11.77	8.69	8.75	7.88	9.12	10.01
MnO	0.16	0.15	0.11	0.16	0.15	0.18	0.18	0.16	0.18	0.15	0.15	0.15	0.16	0.17
MgO	1.06	0.60	0.66	5.30	5.56	3.74	3.44	5.53	3.15	5.68	3.40	3.46	5.20	5.89
CaO	3.57	2.90	2.63	9.84	10.77	8.19	7.96	11.45	7.84	12.08	10.01	7.71	10.21	10.60
Na_2O	5.04	5.02	5.61	3.26	2.19	3.00	2.97	1.86	3.00	1.74	2.57	3.39	2.48	2.20
K_2O	1.19	1.41	1.40	0.28	0.32	0.51	0.65	0.24	0.55	0.63	0.44	0.53	0.50	0.33
P_2O_5	0.18	0.11	0.10	0.11	0.10	0.13	0.15	0.07	0.13	0.14	0.09	0.12	0.11	0.09
LOI	1.18	0.35	2.15	0.48	0.48	0.33	0.63	0.12	1.03	0.06	0.76	0.75	−0.19	−0.04
Total	98.21	99.18	97.36	99.79	99.30	99.28	98.99	99.14	99.10	99.52	99.08	99.21	99.26	98.84
Mg#	32.6	24.2	32.2	54.5	56.5	39.7	38.0	54.0	35.5	57.4	44.5	47.5	54.0	54.8

Volcano	Kuiwai		Ngatorirangi						Sonne					
Lat.	33°10.0′ S	33°07.7′ S	33°43.9′ S	33°43.9′ S	33°44.1′ S	33°42.3′ S	33°45.2′ S	33°45.2′ S	34°04.0′ S	34°04.3′ S	34°02.0′ S	34°02.0′ S	34°00.8′ S	34°01.4′ S
Long.	179°58.0′ W	179°56.6′ W	179°49.8′ E	179°49.8′ E	179°49.8′ E	179°51.0′ E	179°48.3′ E	179°48.3′ E	179°35.2′ E	179°35.2′ E	179°36.6′ E	179°36.6′ E	179°31.9′ E	179°33.4′ E
Depth (mbsl)	821	1806	446	446	555	1479	1500	1500	1040	1088	1976	1976	2013	1271
Sample	32-01	33-01	19-01	19-02	20-02	21-01	24-04	24-08	09-01	10-01	11-01	11-03	14-01	88-01
SiO_2	51.42	52.67	54.60	51.93	52.64	51.91	54.84	57.15	65.80	65.03	61.99	68.69	52.00	52.40
TiO_2	0.78	0.75	1.12	0.84	0.90	0.86	0.79	0.70	0.78	0.79	0.82	0.60	0.77	0.99
Al_2O_3	16.88	16.79	14.78	18.84	16.12	17.37	18.44	16.53	14.49	14.32	14.86	14.41	17.17	16.94
Fe_2O_3	10.35	10.63	12.26	9.85	11.08	10.71	8.49	7.73	6.06	6.12	7.02	4.77	10.09	12.47
MnO	0.17	0.18	0.19	0.1	0.17	0.17	0.14	0.15	0.16	0.16	0.16	0.13	0.17	0.19
MgO	5.18	4.89	4.09	3.86	4.90	4.41	3.16	4.33	1.31	1.43	2.64	0.98	4.76	4.06
CaO	11.11	10.49	8.66	10.99	10.29	10.76	9.86	9.19	4.80	4.80	6.49	4.11	10.48	9.95
Na_2O	2.37	2.36	2.89	2.49	2.35	2.44	2.85	3.12	4.24	4.46	3.54	4.45	2.47	2.61
K_2O	0.29	0.34	0.44	0.32	0.36	0.34	0.44	0.44	0.80	0.77	0.71	0.85	0.69	0.33
P_2O_5	0.09	0.08	0.12	0.09	0.10	0.10	0.11	0.14	0.21	0.23	0.18	0.17	0.14	0.11
LOI	0.28	0.51	0.98	−0.31	−0.18	−0.48	−0.02	−0.18	0.53	1.38	0.92	−0.11	1.01	−0.10
Total	98.92	99.69	99.15	99.36	98.91	99.07	99.12	99.48	99.18	99.49	99.33	99.05	99.75	99.95
Mg#	50.8	48.7	40.7	44.7	47.7	45.9	43.4	53.6	30.8	32.5	43.7	29.7	49.3	40.1

Volcano	Sonne			Kibblewhite				Yokosuka		Rapuhia		Giljanes	
Lat.	34°04.7′ S	34°07.0′ S	34°07.0′ S	34°34.3′ S	34°34.3′ S	34°29.4′ S	34°41.2′ S	34°42.5′ S	34°42.5′ S	34°46.6′ S	34°46.6′ S	34°46.5′ S	34°46.5′ S
Long.	179°29.0′ E	179°25.6′ E	179°25.6′ E	179°15.8′ E	179°15.9′ E	179°14.2′ E	179°18.2′ E	178°34.3′ E	178°34.3′ E	178°30.4′ E	178°30.4′ E	178°34.8′ E	178°34.8′ E
Depth (mbsl)	2405	1841	1841	1134	1174	1438	1642	1144	1144	798	798	790	790
Sample	90-01	91-01	91-04	03-01	05-01	94-02	98-02	102-01	102-03	101-01	101-03	100-01	100-02
SiO_2	49.54	54.72	51.12	55.50	65.42	50.42	49.96	64.34	62.72	53.57	65.28	0.70	59.08
TiO_2	0.55	0.67	0.60	1.03	0.66	0.93	0.41	0.77	0.80	1.26	0.63	0.01	0.93
Al_2O_3	14.02	16.79	14.57	16.62	14.80	17.99	9.31	15.32	16.05	16.36	15.36	0.08	16.06
Fe_2O_3	9.65	8.84	8.22	9.20	5.31	9.57	8.70	4.27	4.50	7.37	3.96	0.40	7.03
MnO	0.16	0.15	0.21	0.21	0.14	0.16	0.15	0.11	0.11	0.14	0.12	61.82	0.15
MgO	9.88	0.12	6.35	3.25	1.60	5.73	16.16	1.19	1.32	6.59	1.20	3.00	2.81
CaO	13.30	9.85	10.14	7.31	4.18	11.66	13.47	3.82	4.20	8.57	3.26	1.72	6.45
Na_2O	1.61	2.28	1.75	3.81	4.44	2.58	1.11	4.40	4.44	3.75	5.19	2.34	4.00
K_2O	0.34	0.46	2.36	0.97	1.74	0.33	0.20	2.22	1.97	1.01	2.12	1.50	1.59
P_2O_5	0.09	0.09	0.32	0.25	0.16	0.13	0.05	0.21	0.22	0.29	0.19	0.07	0.26
LOI	0.20	0.74	3.53	1.61	1.09	0.04	0.11	2.90	2.87	0.38	1.55	22.22	0.65
Total	99.34	99.71	99.17	99.76	99.54	99.54	99.63	99.55	96.33	99.29	99.17	93.86	98.36
Mg#	67.8	54.4	61.4	42.1	38.3	55.2	79.3	36.5	37.7	64.8	38.4	–	45.2

All samples prefixed by TAN0205. Latitude, longitude and depth are mid-points of the dredge track. Analyses completed by XRF, and the loss on ignition (LOI), are reported in wt.%. Mg#=100*[Mg^{2+} / (Mg^{2+} Fe^{2+})] after setting Fe_2O_3/FeO=0.15.

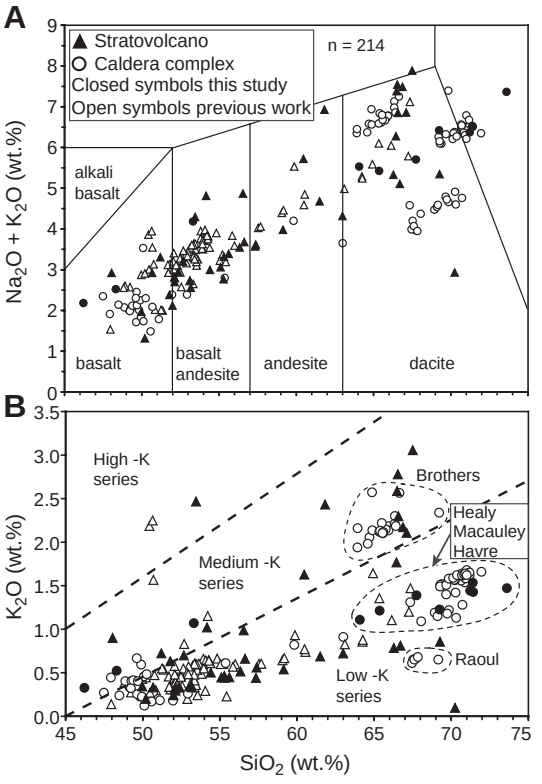

Fig. 18. (A) Total alkali vs. silica and (B) K_2O vs. SiO_2 plots of southern Kermadec arc lavas (whole-rock analyses, anhydrous normalized). Data from this study (30°–35° S sector; closed symbols), and previous studies (south of 35° S, and Raoul and Macauley Islands; open symbols) (Gamble et al., 1993b, 1995, 1996, 1997; Wright and Gamble, 1999; Haase et al., 2002; Christie, 2002; Smith et al., 2003a). Rock classification in (A) and boundaries for the low and medium-K fields in (B) are from Le Bas et al. (1986) and Gill (1981), respectively.

those calculated for the Izu-Bonin arc (Tamura and Tatsumi, 2002), although silicic lavas in the Kermadec arc are predominantly dacite rather than rhyolite. Dacite and rhyolite account for ~30% by volume of Kermadec lavas, basalt–basaltic andesite total ~61%, and intermediate lavas (57–63 wt.% SiO_2) a mere ~9%.

The genesis of silicic magmas in intra-oceanic arcs remains an outstanding petrogenetic issue. Modelling has demonstrated that appropriate major and trace element compositions can be generated by fractional crystallization from a parental basaltic magma (e.g. Ewart et al., 1973; Woodhead, 1988; Pearce et al., 1995). However, similar compositions can also be generated by dehydration melting of basaltic or andesitic sub-arc crust (e.g. Beard, 1995; Rapp and Watson, 1995; Tamura and Tatsumi, 2002). Key factors that favour a major role for crustal anatexis in dacitic magma generation beneath Raoul and Macauley volcanoes include the large volumetric proportion of dacite relative to basalt–basaltic andesite, paucity of intermediate lavas, the sparsely phyric to aphyric nature of the dacite, and unique trace element ratios for each dacite batch erupted at a single volcanic centre that cannot be reconciled with a common mafic parental magma or fractionating magma–crystal assemblage (Worthington, 1998; Smith et al., 2003a,b). Our results reinforce and extend these observations throughout the central and southern Kermadec arc (30°–36°30′ S). Sparsely phyric silicic lavas represent ~30% by volume of the constructed arc (Fig. 20). Dacite from different volcanoes exhibits major yet random changes in composition with latitude (e.g. by a factor of ~2 in K_2O content between the adjacent Brothers and Healy volcanoes), whereas mafic lava compositions show no correlation with latitude (Fig. 18B).

Silicic and bimodal volcanism along the mapped ~720 km section of arc front at 30°–36°30′ S is restricted to sectors where the base of the volcanic constructs is shallower than 2700 m, and typically at 1500–2500 m (Fig. 21A). In contrast, except for Sonne which is located on the border between shallow and deep arc sectors, only basalt and basaltic andesite were recovered from the deeper central arc segment where basal edifice water-depths are 3200–3500 m. Variations in K_2O content along the arc front mimic those in SiO_2 (Fig. 21B), but provide no evidence of any change in K_2O content of the most mafic lavas with latitude or depth (excluding the higher K_2O contents of those volcanoes located behind the arc front). Thus, silicic magmatism is evidently enabled in areas of higher standing, thickened arc crust, and the process that generates silicic magmas also leads to a broad spectrum of K_2O contents at high SiO_2 compositions.

We contend that these observations are most consistent with dacite genesis by crustal anatexis. Re-establishment of a stable volcanic arc front following rifting of the former proto-Kermadec–Colville arc and opening of the Havre Trough probably took place

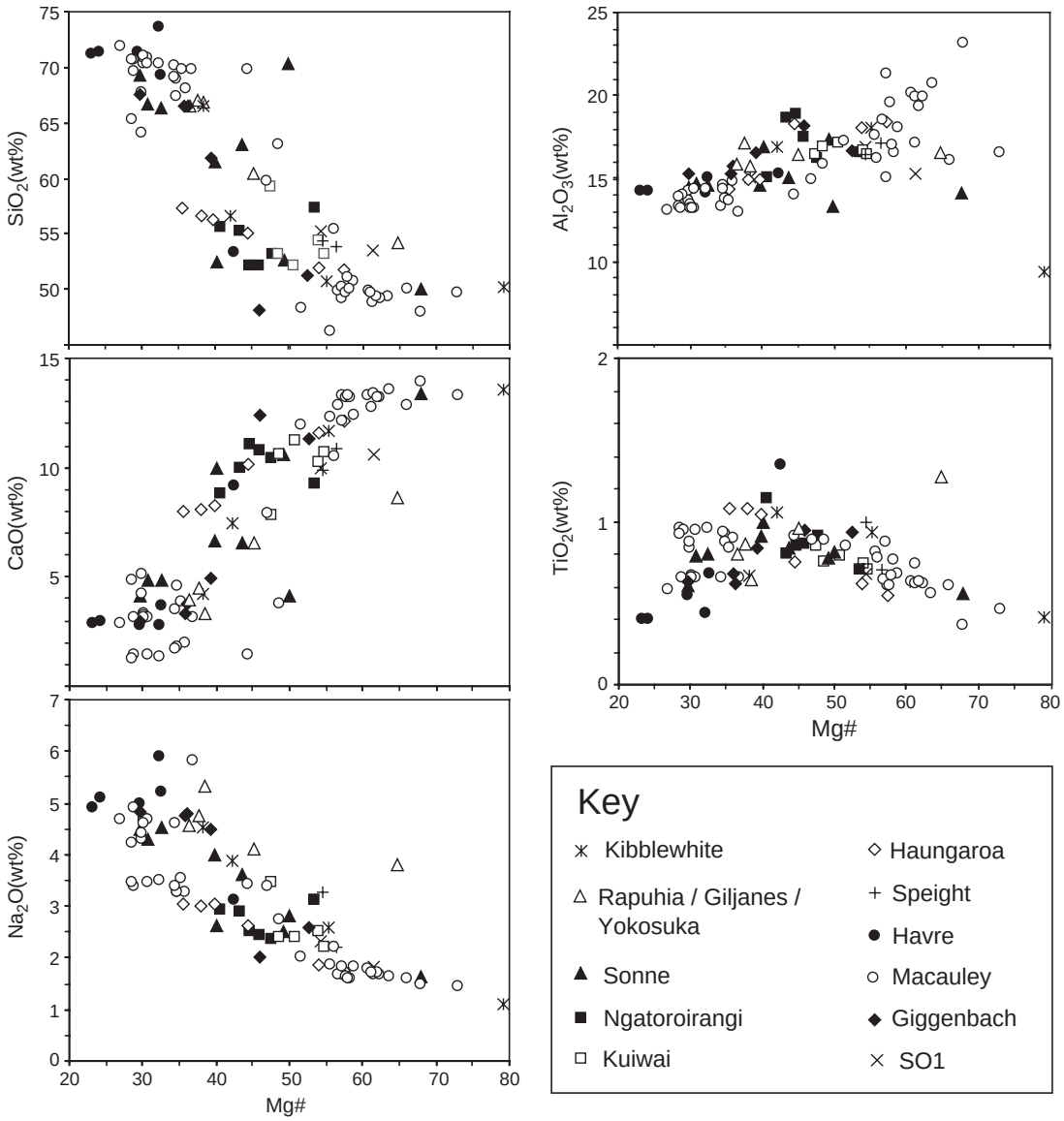

Fig. 19. Plots of selected major elements (normalized to 100% on an anhydrous basis) for the 30°–35° S volcanoes against Mg-number (Table 2). Data includes lavas from Macauley Island (Smith et al., 2003a).

within the last 1–2 Ma (Wright et al., 1996). At that stage, both the eruption of mafic magmas to build arc edifices and thermal conditioning of the sub-arc crust through magmatic underplating and/or intrusion would have commenced. The base of thick crust is inherently at a higher initial temperature than that of thin crust, and thick crust will also provide a greater obstacle to ascending magmas (thus enhancing underplating and the stagnation of intruding magmas). Therefore, the thermal evolution of thick crust should proceed more rapidly than that of thin crust, leading us to predict that silicic volcanism will occur first in high-standing arc sectors such as those featuring Brothers and Healy or Raoul and Macauley (Fig.

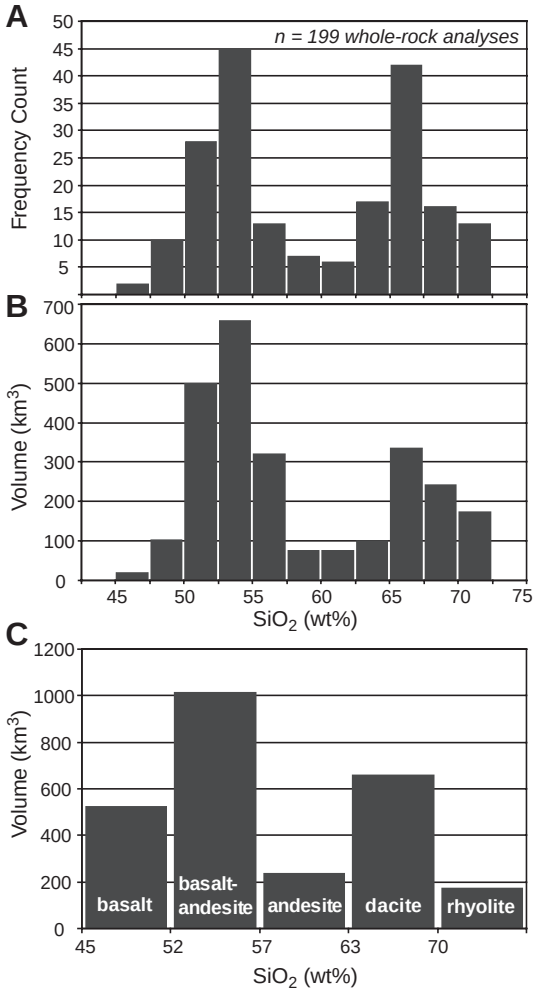

Fig. 20. Frequency and volume-weighted histograms of SiO_2 content (on an anhydrous basis) for the 30°–36°30′ S sector of the Kermadec arc. Data sources and edifice volumes are given in Fig. 18 and Table 1, respectively.

21). In contrast, crustal anatexis will take longer to commence in the arc sector with thinner crust between 32°20′ and 34°10′ S, where Sonne, Ngatoroirangi, Kuiwai, Haungaroa, and Oliver volcanoes remain in the youthful stage of arc construction and only basalt–basaltic andesite has yet been erupted (Fig. 21). Similar models of spatial and temporal evolution for arc magmatism on continental crust, at scales of 10^6 yr and arc sectors a few hundred kilometers long, have been proposed for the Taupo Volcanic Zone (Wilson et al., 1995; Price et al., 2005).

6.2. Kermadec silicic caldera volcanism

Caldera-forming volcanism associated with the silicic magmatism is also recognized increasingly within intra-oceanic arcs (e.g. Yuasa et al., 1991; Crawford et al., 1988; Fiske et al., 2001), including the Tonga and Kermadec (Lloyd et al., 1996; Worthington et al., 1999; Wright and Gamble, 1999) systems. For the southern Kermadec arc, the distribution of calderas essentially mirrors the lateral variation in arc topography and lava geochemistry. The larger calderas (i.e. Raoul, Macauley, Havre, Brothers, Healy with diameters >3 km) coincide with the shallower and more silicic arc segments (Fig. 21). The sole exception is Sonne, where three nested calderas at the summit (the largest <2.6 km in diameter; Fig. 15) are associated with pumiceous dacite (Table 2, Appendix A). Although the genesis of these silicic calderas is equivocal (e.g. incremental collapse associated with episodic magma withdrawal at Brothers—Wright and Gamble, 1999), the predominant mode of formation is interpreted as mass discharge, submarine pyroclastic eruptions with syn-eruptive caldera collapse (e.g., Macauley and Healy—Lloyd et al., 1996; Wright et al., 2003). Hence, the shallower arc segments are zones where both thickened crusts may melt to produce silicic magma and the reduced hydrostatic load allows subsequent magma vesiculation and fragmentation that initiates and sustains pyroclastic eruptions and caldera formation. The depth limit of pyroclastic eruptions at Healy has been estimated at 900–1000 m, and ~1200 m for the more general case of a volatile-rich silicic melt assuming 70% vesicularity to induce fragmentation (Wright et al., 2003).

Observational data for the central-southern Kermadec arc are mostly consistent with this interpretation, and reveal three distinct caldera/crater groupings (Fig. 22). Unequivocal calderas are associated with the eruption of magma containing >70 wt.% SiO_2, have diameters of variable sizes that range up to at least ~11 km, and have post-eruptive rim water-depths of ~1200–1400 m (though the pre-eruption topography was presumably shallower). A second group of more equivocal “calderas”, including Brothers (Wright and Gamble, 1999), is associated with lava compositions in the range 60–70 wt.% SiO_2, smaller rim diameters that are mostly <2 km, and rim water-depths of

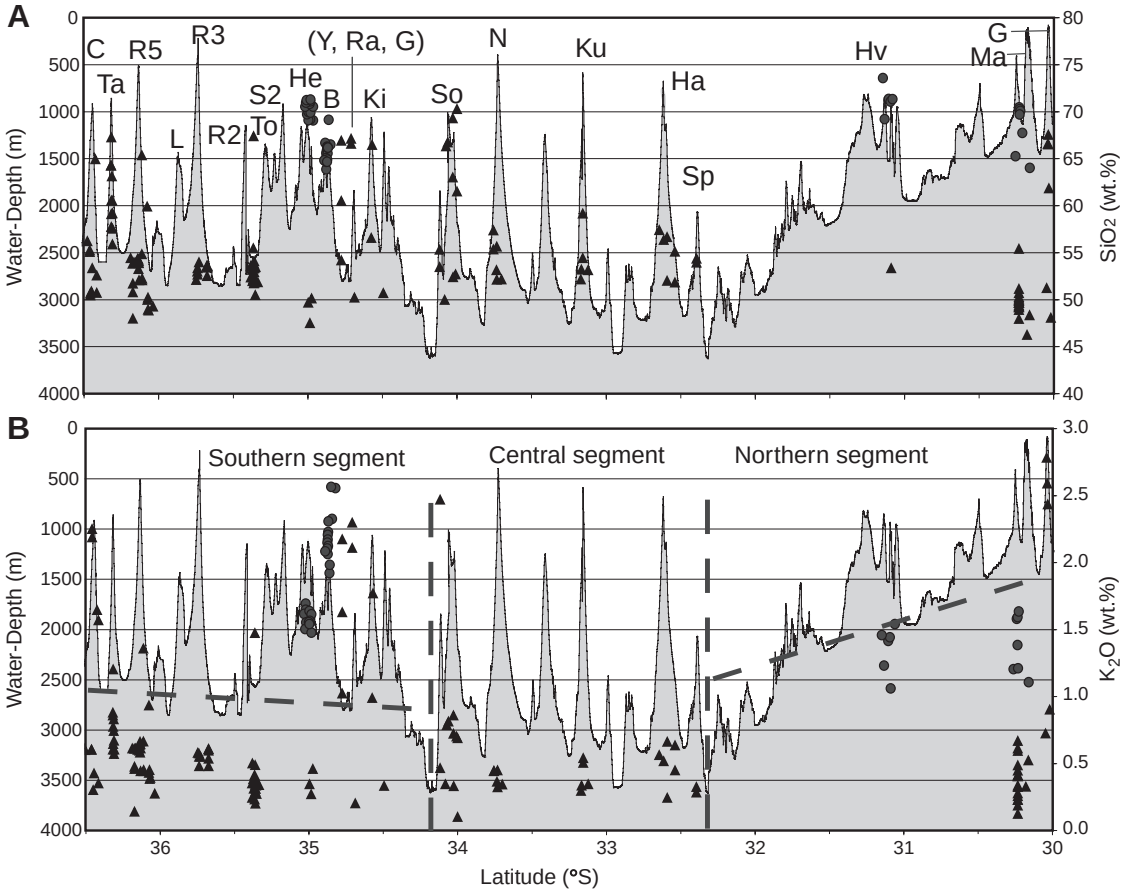

Fig. 21. Variation of lava chemistry (right axis, normalized to total 100% on an anhydrous basis) for SiO_2 (A) and K_2O (B) plotted on a lateral bathymetry profile (left axis) of the southern Kermadec arc (30°–36°30′ S). Volcano names; Clark (C), Tangaroa (Ta), Rumble V (R5), Rumble III (R3), Rumble II (East and West) (R2), Thompson (To), Silent II (S2), Healy (He), Brothers (B), Rapuhia (Ra), Yokosuka (Y), Giljanes (G), Kibblewhite (Ki), Sonne (So), Ngatoroirangi (N), Kuiwai (Ku), Haungaroa (Hu), Speight (Sp), Havre (Hv), Macauley (M), and Giggenbach (G). Rapuhia, Yokosuka, and Giljanes volcanoes are projected from 45 km west of the arc front onto the profile. Triangles and circles are basalts–andesites and dacites–rhyolites, respectively.

mostly <1500–1400 m (Fig. 22). Some of these "calderas" (e.g., Sonne and Kibblewhite) are probably true syn-eruptive catastrophic collapses associated with small dacitic eruptions at shallow to medium water-depths. Conversely, other "calderas" (e.g., Yokosuka) are unlikely to have been syn-eruptive catastrophic collapses as water-depths of >2000 m are involved. Where the edifice is basaltic and the water depth is ≥1000 m (e.g. Haungaroa), then the summit structures are possibly craters or explosion pits. Nevertheless, the general parameters for sustained submarine pyroclastic eruption hold where water-depths are <1000 m and magmas have >70 wt.% SiO_2 combined with water contents of 5–6 wt.% (Wright et al., 2003).

6.3. Kermadec volcano sector collapse

Large-scale slope failure, but principally landslides and debris avalanches, are increasingly recognized on the flanks of both fully and partially submerged arc volcanoes (e.g., Deplus et al., 2001). Various causal mechanisms have been proposed for flank slope failure (Siebert, 1984; Thouret, 1999), including hydrothermal alteration and rock weakening (Lopez and Willaims, 1993), formation of dip

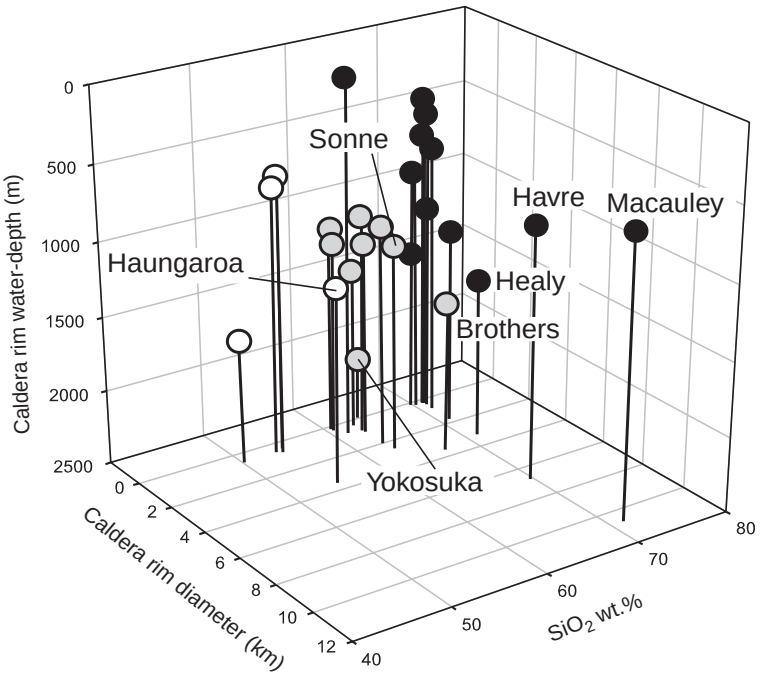

Fig. 22. Three-dimensional plot of the Kermadec arc volcanoes with caldera diameter and post-eruptive rim water-depth, against SiO_2 wt.% (as the average of the five most silicic whole-rock analyses for each volcano).

slopes with intercalating competent lavas and unconsolidated volcaniclastics, extensional rift zones and/or dike swarms that parallel the local stress field, and sub-volcanic basement flank "spreading" (Cecchi et al., 2004), with the latter being either symmetric or asymmetric.

For the Kermadec volcanoes, the imprint of extensional back-arc tectonism on edifice structure (with structural control of faults, dikes, and flank rifts) dictates that initiated flank 'spreading' is asymmetric. Asymmetric 'spreading' is more conducive to the sector collapse (van Wyk de Vries and Francis, 1997) with the development of characteristic deep-seated horse-shoe sector collapses that are preferentially orientated parallel to the Havre Trough extension (e.g., Kuiwai, Sonne, and Kibblewhite volcanoes, Figs. 12, 15, and 16)), though not exclusively so (e.g., Giggenbach and Haungaroa volcanoes, Figs. 4 and 10). Preliminary estimates show such collapse structures can vary up to at least ~4 km^3 in volume, though these probably represent multiple failures rather than single catastrophic events. Conversely, the high-resolution 30 kHz data also image shallow failures, typically less than 50 m thick in relief, and possibly represent syn-eruptive slip failures.

7. Conclusions

Integrated multibeam mapping, seafloor photography, rock dredging, and whole-rock geochemistry provide a first order definition of the present-day submarine Kermadec arc at 30°–35° S. Twenty-two volcanoes with diameters >5 km, were discovered or completely mapped for the first time. Included are Giggenbach, Macauley, Havre, Haungaroa, Kuiwai, Ngatoroirangi, Sonne, Kibblewhite and Yokosuka volcanoes which have basal diameters in the range 10–35 km. For each edifice, volcano morphology and structure, surficial deposits, lava flow fields, distribution of sector collapses, and lava compositions were determined. Havre and Macauley are significant caldera volcanoes. For the latter, Macauley Island represents <5% of a large submerged volcanic complex. Concentric outer flank ridges on both calderas are interpreted as recording mega-bedforms associated

with eruptive density flows and associated edifice foundering. Likewise, the stratovolcanoes reveal complex volcanic histories characterized by repeated cycles of tectonically controlled construction and sector collapse, which can include small, crest-nested calderas (e.g. on Sonne) and extensive basaltic flow fields (e.g. on Haungaroa).

These new data, combined with existing data from the southernmost part of the arc (e.g., Gamble et al., 1996; Wright and Gamble, 1999) provide an overview of the spatial distribution and magmatic heterogeneity along ~780 km of the Kermadec arc. Coincident changes in arc elevation and composition define three volcano–tectonic segments. A central deeper section is characterized by basement elevations of >3200 m water-depth and relatively simple stratovolcanoes that predominantly erupt low-K series basalt–basaltic andesite. In contrast, the adjoining segments have higher basement elevations (typically <2500 m water-depth), multiple-vent volcanic centres, and erupt sub-equal proportions of basaltic and dacitic magma. The association of silicic magmas with higher basement elevations (and hence interpreted thicker crust), coupled with significant inter- and intra-volcano heterogeneity of the silicic lavas but not the basaltic lavas, is interpreted as evidence that dehydration melting of the Kermadec crust plays a significant role in dacite magma genesis. Conversely, beneath the deeper central arc segment the thermal requirements for crustal anatexis of the thinner (initially cooler) crust have not yet been met.

Silicic calderas with diameters >3 km are restricted to the shallower and more compositionally evolved arc segments. The dominant mode of large caldera formation is interpreted as mass-discharge pyroclastic eruption with syn-eruptive collapse. Hence, beneath the shallower arc segments the thicker crust may undergo dehydration melting to produce volatile-enriched silicic magmas and a reduced hydrostatic load allows subsequent magma vesiculation and fragmentation to initiate and sustain pyroclastic eruptions. The general parameters for submarine pyroclastic eruption hold where water-depths are <1000 m and erupting magmas have 5–6 wt.% water and >70 wt.% SiO_2.

Acknowledgments

Thanks are due to officers and crew of *RV Tangaroa* for the successful TAN0205 voyage, with special thanks to R. Garlick and J. Mitchell for the EM300 acquisition and processing. Thanks are also due to A. Weinkopf and P. Appel for assistance with the geochemical analyses undertaken at University of Kiel. The figures were produced by E. Mackay, and comments by Lionel Carter and reviews by Steve Carey and Jim Cole improved the final manuscript. This work was funded by the Foundation for Research Science and Technology (New Zealand) under contract C01X0203 and the Bundesministerium für Bildung und Forschung.

Appendix A. Sample locations and synoptic petrography

Abbreviations: tr—trace, phenos—phenocrysts, plag—plagioclase, pyx—pyroxene, vesics—vesicles

Giggenbach
- TAN0205-65; central cone in summit crater; 182–103 m water-depth
  - 65-01; blue-grey dacite; phenos—tr plag to 2 mm; 20% lighter devitrification zones to 2 mm; dense jointed flow
- TAN0205-67; uppermost southeast flank; 795–414 m water-depth
  - 67-04; blue-grey basalt; phenos—tr plag to 2 mm; 5% vesics
- TAN0205-72; active east–west aligned volcanotectonic zone west of Giggenbach; 1161–960 m water-depth
  - 72-01; black dacite; phenos—10% plag to 2 mm; 5% vesics flow stretched to 5 mm long; massive block
- TAN0205-73; crest of GI4 cone; 1086–872 m water-depth
  - 73-01; black andesite; phenos—tr plag to 1 mm; non-vesicular pillow sector
- TAN0205-74; western upper flank of main edifice; 165–141 m water-depth
  - 74-01; pale blue dacite; phenos—aphyric; 20% vesics both elongate and flow aligned to 3 mm

TAN0205-77; edifice crest of satellite GI1 volcano; 883–682 m water-depth
77-02; black basalt; phenos—10% to 20% plag to 5 mm (banded); 10% vesics sub-mm to 5% at 5 mm

Macauley
TAN0205-55; summit of intra-caldera Macauley cone; 504–480 m water-depth
55-01; black dacite; phenos—tr plag to 2 mm, 20% vesics small to 3 mm elongate and flow aligned
TAN0205-60; post-caldera cone on outer northern caldera rim; 751–636 m water-depth
60-01; grey-black dacite; phenos—5% plag to 1 mm and tr pyx; flow aligned vesics; dense massive flow
TAN0205-62; post-caldera flow on outer mid-southwest caldera flank; 1096–980 m water-depth
62-01; dark grey dacite; phenos—aphyric; 5% vesics up to elongate 5 mm; dense massive block
TAN0205-63; crestal cone atop Lloyd dome; 157–88 m water-depth
63-01; black basalt; phenos—aphyric; scoriaceous block with 50% vesics small to 1 mm
TAN0205-64; crest of Lloyd dome; 328–287 m water-depth
64-01; black basalt; phenos—aphyric; weakly scoriaceous block with abundant sub-mm vesics

Havre
TAN0205-45; inner northeast caldera rim; 1112–941 m water-depth
45-02; blue-grey dacite; phenos—10% plag and 10% pyx both to 2 mm; flow-banded non-vesicular block
TAN0205-46; inner northwest caldera rim; 947–934 m water-depth
46-01; black dacite; phenos—tr plag to 1 mm; 20% vesics to 1 mm and locally scoriaceous
46-03; grey basalt; phenos—5% plag to 3 mm (mostly <1 mm); 5–10% vesics to 2 mm
TAN0205-47; southeast caldera rim; 841–776 m water-depth
47-03; black dacite; phenos—10% plag to 2 mm; 10% vesics elongate to 1 cm; dense flow block
TAN0205-49; outer mid-northwestern flank; 1272–1248 m water-depth
49-01; blue-grey dacite; phenos—aphyric; few small vesics to <1 mm; dense jointed flow block
TAN0205-51; outer mid-southeast flank; 1144–768 m water-depth
51-01; blue dacite; phenos—aphyric; 5-10% vesics small to flow aligned 1 cm vugs; pumiceous with sub-mm devitrification banding

Oliver
TAN0205-43; edifice crest; 2363–2317 m water-depth
43-01; grey basaltic andesite; phenos—tr plag and pyx to 2 mm; 5% vesic <1 mm; ropey pillow with 2–3 mm glassy rind
43-03; black basaltic andesite; phenos—15% plag and tr pyx both to 2 mm; 15% vesics to 3 mm; glassy rind

Haungaroa
TAN0205-34; cone on western caldera rim; 888–741 m water-depth
34-01; black basaltic andesite; phenos—aphyric; 5% vesics strongly flow aligned to 1 cm long; 2–3 mm glassy rind
TAN0205-37; mid-flank of northern ridge spur; 1366–968 m water-depth
37-01; black basaltic andesite; phenos—tr plag; 5% vesics small to flow aligned 2 cm long
37-03; blue-grey basalt; phenos—20% plag to 3 mm and 5% pyx to 3 mm; 5% vesics to 4 mm
TAN0205-38; lower southeast flank; 2327–2044 m water-depth
38-01; black basaltic andesite; phenos—5% plag to 2 mm; 5% vesicles small to 2 mm, pillow with 1–5 mm glassy rind and 3.5 cm core void
TAN0205-82; northern mid-flank on older lava field sequences; 2312–1958 m water-depth
82-01; black basalt; phenos—15% plag to 4 mm and tr pyx to 2 mm; inhomogeneous porphyritic texture; 15% vesics to 2 mm
82-03; black basaltic andesite; phenos—10% plag to 3 mm and tr pyx; 5% vesicles to 5 mm

Kuiwai
TAN0205-27; edifice crest; 667–613 m water-depth
27-01; blue-grey andesite; phenos—tr plag to 2 mm; pumiceous with 15% vesics small to 2 cm vugs; devitrification banding
27-04; black basaltic andesite; phenos—20% plag to 3 mm and tr pyx; 10% vesics small to 1 cm vugs
TAN0205-28; edifice crest of satellite KU1 cone; 1344–1183 m water-depth
28-01; black basalt; phenos—20% plag mostly to 1 mm but rarely to 2 mm and 5% pyx to 2 mm; 20% vesics small to 6 cm vugs
TAN0205-32; uppermost southwest flank to main edifice; 999–643 m water-depth
32-01; black basalt; phenos—10% plag to 2 mm; 10% vesics small to flow aligned 1 cm long
TAN0205-33; lower northeast flank; 2090–1522 m water-depth
33-01; blue-grey basalt; phenos—15% plag to 3 mm; 10% vesics elongate to 2 mm; pillow with 2 mm glassy rind

Ngatoroirangi
TAN0205-19; edifice crest; 420–471 m water-depth
19-01; black basaltic andesite; phenos—tr plag to 3 mm; 10% vesics to 6 cm long vugs
19-02; black basalt; phenos—25% plag to 5 mm; 5% vesics to 5 mm
TAN0205-20; upper southeast flank; 490–619 m water-depth
20-02; black basalt; phenos—10% plag to 3 mm and tr pyx to 5 mm; 5% vesics to 2 cm

TAN0205-21; mid-northeast flank; 1330–1627 m water-depth
21-01; black basalt; phenos—15% plag to 3 mm; 15% vesics small grading to 1.5 cm vugs
TAN0205-24; mid-southwest flank; 1600–1400 m water-depth
24-04; black basaltic andesite; phenos—20% plag to 2 mm and tr pyx; non-vesicular
24-08; grey andesite; phenos—10% plag to 2 mm and tr pyx; 10% elongated vesics; dense flow

Sonne
TAN0205-09; edifice crest; 1058–1022 m water-depth
09-01; black dacite; phenos—tr plag to 2 mm; non-vesicular
TAN0205-10; edifice crest; 1121–1055 m water-depth
10-01; grey dacite; phenos—tr plag to 1 mm; pumiceous with 10% vesics flow aligned to 1 cm
TAN0205-11; mid-northern flank; 2106–1846 m water-depth
11-01; black andesite; phenos—5% plag to 3 mm and tr pyx; 10% vesics flow aligned to 1 cm
11-03; blue-grey dacite; phenos—tr plag; 5% small vesics
TAN0205-14; lower northwest flank; 2138–1887 m water-depth
14-01; grey basalt; phenos—20% plag to 2 mm, 5% olivine to 1 mm, 5% pyx to 2 mm; non-vesicular
TAN0205-88; outer rim of breached northwest caldera; 1327–1214 m water-depth
88-01; black basalt; phenos—20% plag to 4 mm; 20% vesics small to spherical 3 mm but also flow aligned to 2.5 cm
TAN0205-90; mid-southwest flank; 2495–2314 m water-depth
90-01; blue-grey basalt; phenos—10% pyx to 2 mm; 25% vesics to 3 mm; pillow with 3 mm glassy rind
TAN0205-91; crest of satellite SO1 cone; 1885–1797 m water-depth
91-01; black basaltic andesite; phenos—10% plag to 2 mm and 5% pyx to 3 mm; 5% vesics to 1 cm
91-04; grey basalt; phenos—10% pyx to 4 mm and tr plag to 1 mm; 5% vesics to 8 mm

Kibblewhite
TAN0205-03; edifice crest; 1300–968 m water-depth
03-01; green basaltic andesite; phenos: 5% pyx rods to 1 mm; pillow with granular glass core with 20% void space
TAN0205-05; uppermost northern flank; 1344–1003 m water-depth
05-01; blue-grey dacite; phenos—5% plag to 2 mm and 2% pyx to 2 mm; 1–2 mm devitrification banding
TAN0205-94; edifice crest of satellite KI1 cone; 1537–1338 m water-depth
94-02; blue-grey basalt; phenos—15% plag to 2 mm; 20% vesics 3 mm at pillow core to <1 mm at crust
TAN0205-98; edifice crest of satellite KI4 cone; 1713–1570 m water-depth
98-02; black basalt; phenos—10% pyx to 1 cm and 5% olivine to 1 cm (30% pyx along base of pillow); 5% vesics; drained 3 cm vugs at pillow core

Yokosuka
TAN0205-102; edifice crest; 1172–1115 m water-depth
102-01; pale blue dacite; phenos—tr plag to 2 mm and tr hornblende/pyx to 0.5 mm; 5% vesics
102-03; grey andesite; phenos—10% plag to 2 mm; 5% vesics to 3 mm

Rapuhia
TAN025-101; edifice crest; 825–771 m water-depth
101-01; black basaltic andesite; phenos—tr plag to 3 mm and tr pyx to 2 mm; 10% vesics to 5 mm
101-03; blue-grey dacite; phenos—10% hornblende to 2 mm, 5% plag to 3 mm and tr pyx to 2 mm; non-vesicular jointed block

Giljanes
TAN0205-100; edifice crest; 850–730 m water-depth
100-01; black to grey MnOx; bedded with 3 mm to 1 cm thick MnOx beds separated by volcaniclastic sands
100-02; black andesite; phenos—25% plag to 2 mm and 5% pyx to 2 mm; 5% vesics to 3 mm

References

Aramaki, S., Ui, T., 1978. Major element frequency distribution of Japanese Quaternary volcanic rocks. Bull. Volcanol. 41, 390–407.

Baker, E.T., Feely, R.A., de Ronde, C.E.J., Massoth, G.J., Wright, I.C., 2003. Submarine hydrothermal venting on the southern Kermadec volcanic arc front (offshore New Zealand): location and extent of particle plume signatures. In: Larter, R.D., Leat, P.T. (Eds.), Intra-Oceanic Subduction Systems: Tectonic and Magmatic Processes, Geol. Soc. London Spec. Pub., vol. 219, pp. 141–161.

Ballance, P.F., Ablaev, A.G., Pushchin, I.K., Pletnev, S.P., Birylina, M.G., Itaya, T., Follas, H.A., Gibson, G.W., 1999. Morphology and history of the Kermadec trench–arc–backarc basin–remnant arc system at 30 to 32° S: geophysical profile, microfossil and K–Ar data. Mar. Geol. 159, 35–62.

Beard, J.S., 1995. Experimental, geological, and geochemical constraints on the origins of low-K silicic magmas in oceanic arcs. J. Geophys. Res. 100 (15), 15593–15600.

Bird, P., 2003. An updated digital model of plate boundaries. Geochem. Geophys. Geosyst. 4 (3). doi:10.1029/2001GC000252.

Brothers, R.N., Martin, K.R., 1970. The geology of Macauley Island, Kermadec group, southwest Pacific. Bull. Volcanol. 34, 330–346.

Caress, D.W., 1991. Structural trends and backarc extension in the Havre Trough. Geophys. Res. Lett. 18, 853–856.

Cecchi, E., van Wyk de Vries, B., Lavest, J.-M., 2004. Flank spreading and collapse of weak-cored volcanoes. Bull. Volcanol. 67, 72–91.

Christie, R.H.K., 2002. The petrology, geochemistry and petrogenesis of volcanic rocks from the southern Kermadec oceanic island arc, South West Pacific. unpub. MSc Thesis, Victoria University of Wellington.

Cole, J.W., 1986. Distribution and tectonic setting of Late Cenozoic volcanism in New Zealand. In: Smith, I.E.M. (Ed.), Late Cenozoic Volcanism in New Zealand, Roy. Soc. N.Z. Bull., vol. 23, pp. 7–20.

Crawford, A.J., Greene, G.H., Exon, N.F., 1988. Geology, petrology and geochemistry of submarine volcanoes around Epi Island, New Hebrides Island arc. In: Greene, H.G., Wong, F.L. (Eds.), Geology and Offshore Resources of Pacific Island Arcs—Vanuatu Region. Circum-Pacific Counc., Energy Min. Resourc. Earth Sc. Ser., vol. 8, pp. 301–327 (Houston, TX).

de Ronde, C.E.J., Baker, E.T., Massoth, G.J., Lupton, J.E., Wright, I.C., Feeley, R.A., Greene, R.R., 2001. Intra-oceanic subduction-related hydrothermal venting, Kermadec volcanic arc, New Zealand. Earth Planet. Sci. Lett. 193, 359–369.

de Ronde, C.E.J., Faure, K., Bray, C.J., Chappel, D.A., Wright, I.C., 2003. Hydrothermal fluids associated with seafloor mineralisation at two southern Kermadec arc volcanoes, offshore New Zealand. Mineral. Depos. 38, 217–233.

Delteil, J., Ruellan, E., Wright, I.C., Matsumoto, T., 2002. Structure and structural development of the Havre Trough (SW Pacific). J. Geophys. Res. 107 (B7) (10.1029/2001JB000494).

Deplus, C., Le Friant, A., Boudon, G., Komorowski, J.-C., Villemant, B., Harford, C., Ségoufin, J., Cheminée, J.-L., 2001. Submarine evidence for large-scale debris avalanches in the Lesser Antilles Arc. J. Earth Planet. Sci. Lett. 192, 145–157.

Ewart, A., Hawkesworth, C.J., 1987. The Pleistocene–Recent Tonga–Kermadec arc lavas: interpretation of new isotopic and rare earth data in terms of a depleted mantle source model. J. Petrol. 28, 495–530.

Ewart, A., Bryan, W.B., Gill, J.B., 1973. Mineralogy and geochemistry of the younger volcanic islands of Tonga, S.W. Pacific. J. Petrol. 14, 429–465.

Ewart, A., Brothers, R.N., Mateen, A., 1977. An outline of the geology and geochemistry, and the possible petrogenetic evolution of the volcanic rocks of the Tonga–Kermadec–New Zealand island arc. J. Volcanol. Geotherm. Res. 2, 205–250.

Ewart, A., Collerson, K.D., Regelous, M., Wendt, J.I., Niu, Y., 1998. Geochemical evolution within the Tonga–Kermadec–Lau arc–back-arc systems: the role of varying mantle wedge composition in space and time. J. Petrol. 39, 331–368.

Fiske, R., Naka, J., Iizasa, M., Klaus, A., 2001. Submarine silicic caldera at the front of the Izu-Bonin arc, Japan: voluminous seafloor eruptions of rhyolite pumice. Geol. Soc. Amer. Bull. 113, 813–824.

Gamble, J.A., Wright, I.C., 1995. The Southern Havre Trough: geological structure and magma petrogenesis of an active back-arc rift complex. In: Taylor, B. (Ed.), Back-arc Basins: Tectonics and Magmatism. Plenum Press, New York, pp. 29–62.

Gamble, J.A., Smith, I.E.M., Graham, I.J., Kokelaar, B.P., Cole, J.W., Houghton, B.F., Wilson, C.J.N., 1990. The petrology, phase relations and tectonic setting of basalts from the Taupo Volcanic Zone, New Zealand, and the Kermadec Island arc—Havre Trough, SW Pacific. J. Volcanol. Geotherm. Res. 43, 235–270.

Gamble, J.A., Smith, I.E.M., McCulloch, M.T., Graham, I.J., Kokelaar, B.P., 1993a. The geochemistry and petrogenesis of basalts from the Taupo Volcanic Zone and Kermadec Island arc, S.W. Pacific. J. Volcanol. Geotherm. Res. 54, 265–290.

Gamble, J.A., Wright, I.C., Baker, J.A., 1993b. Seafloor geology and petrology of the oceanic to continental transition zone of the Kermadec–Havre–Taupo volcanic arc system, New Zealand. N.Z. J. Geol. Geophys. 36, 417–435.

Gamble, J.A., Wright, I.C., Woodhead, J., McCulloch, M.T., 1995. Arc and back-arc geochemistry in the southern Kermadec arc—Ngatoro Basin and offshore Taupo Volcanic Zone, SW Pacific. In: Smellie, J.L. (Ed.), Volcanism Associated with Extension at Consuming Plate Margins, Geol. Soc. Lond. Spec. Publ., vol. 81, pp. 193–212.

Gamble, J.A., Woodhead, J., Wright, I.C., Smith, I.E.M., 1996. Basalt and sediment geochemistry and magma petrogenesis in a transect from oceanic island arc to rifted continental margin arc: the Kermadec–Hikurangi margin, SW Pacific. J. Petrol. 37, 1523–1546.

Gamble, J.A., Christie, R.H.K., Wright, I.C., Wysoczanski, R.J., 1997. Primitive K-rich magmas from Clark Volcano, southern Kermadec arc: A paradox in the K-depth relationship. Can. Miner 35, 275–290.

Gill, J.B., 1981. Orogenic Andesites and Plate Tectonics. Springer, New York. 390 pp.

Haase, K.M., Worthington, T., Stoffers, P., Garbe-Schöberg, G., Wright, I.C., 2002. Mantle dynamics, element recycling, and magma genesis beneath the Kermadec Arc–Havre Trough. Geochem. Geophys. Geosyst. 3 (11), 1071. doi:10.1029/2002GC000335.

Karig, D.E., 1970. Ridges and basins of the Tonga–Kermadec island arc system. J. Geophys. Res. 75, 239–254.

Kleiner, A., Chance, J., Ching, N., Mitchell, J., Smits, F., Spittal, J., Spillard, R., 2001. A collaborative effort to meet New Zealand's mapping requirements: multibeam echosounder integration, acceptance testing, and Antarctic mapping aboard the research vessel Tangaroa. OCEANS'2001 Conf. Proceed, pp. 1248–1256.

Le Bas, M.J., Le Maitre, R.W., Streckeisen, A., Zanettin, B., 1986. A classification of igneous rocks based upon the alkali–silica diagram. J. Petrol. 27, 745–750.

Le Gonidec, Y., Lamarche, G., Wright, I.C., 2003. Inhomogeneous substrate analysis using EM300 backscatter imagery. Mar. Geophys. Res. 24, 311–327.

Leat, P.T., Smellie, J.L., Millar, I.L., Larter, R.D., 2003. Magmatism in the South Sandwich arc. In: Larter, R.D., Leat, P.T. (Eds.),

Intra-Oceanic Subduction Systems: Tectonic and Magmatic Processes, Geol. Soc. London Spec. Pub., vol. 219, pp. 285–313.
Lipman, P., 1997. Subsidence of ash-flow calderas: relation to caldera size and magma-chamber geometry. Bull. Volcanol. 59, 198–218.
Lloyd, E.F., Nathan, S., 1981. Geology and Tephrochronology of Raoul Island, Kermadec Group, New Zealand. N.Z. Geol. Survey Bull., vol. 95. N.Z. Dept. Sci. Ind. Res., Wellington. 105 pp.
Lloyd, E.F., Nathan, S., Smith, I.E.M., Stewart, R.B., 1996. Volcanic history of Macauley Island, Kermadec Ridge, New Zealand. N.Z. J. Geol. Geophys. 39, 295–308.
Lopez, D.L., Willaims, S.D., 1993. Catastrophic volcanic collapse: relation to hydrothermal processes. Science 260, 1794–1796.
Parson, L.M., Wright, I.C., 1996. The Lau–Havre–Taupo back-arc basin: a southward, propagating, multi-stage, evolution from rifting to spreading. Tectonophysics 263, 1–22.
Pearce, J.A., Baker, P.E., Harvey, P.K., Luff, I.W., 1995. Geochemical evidence for subduction fluxes, mantle melting and fractional crystallisation beneath the South Sandwich island arc. J. Petrol. 36, 1073–1109.
Pelletier, B., Dupont, J., 1990. Erosion, accretion, backarc extension and slab length along the Kermadec subduction zone, southwest Pacific. C.R. Acad. Sci. Ser. II 310, 1657–1664.
Pelletier, B., Louat, R., 1989. Seismotectonics and present-day relative plate motions in the Tonga–Lau and Kermadec–Havre region. Tectonophysics 165, 237–250.
Price, R.C., Gamble, J.A., Smith, I.E.M., Stewart, R.B., Eggins, S., Wright, I.C., 2005. An integrated model for the temporal evolution of andesites and rhyolites and crustal development in New Zealand's North Island. J. Volcanol. Geotherm. Res. 140, 1–24.
Ramillien, G., Wright, I.C., 2000. Predicted seafloor topography of the New Zealand region; a nonlinear least squares inversion of satellite altimetry data. J. Geophys. Res. 105 (B5), 16577–16590.
Rapp, R.P., Watson, E.B., 1995. Dehydration melting of metabasalt at 8–32 kbar: implications for continental growth and crust–mantle recycling. J. Petrol. 36, 891–931.
Reyners, M., 1989. New Zealand seismicity 1964–87: an interpretation. N.Z. J. Geol. Geophys. 32, 307–315.
Ruellan, E., Delteil, J., Wright, I.C., Matsumoto, T., 2003. From rifting to active spreading in the Lau Basin–Havre Trough backarc system (SW Pacific): Locking/unlocking induced by seamount chain subduction. Geochem. Geophys. Geosyst. 4 (5), 8909. doi:10.1029/2001GC000261.
Siebert, L., 1984. Large volcanic debris avalanches: characteristics of source areas, deposists, and associated eruptions. J. Volcanol. Geotherm. Res. 22, 163–197.
Smith, I.E.M., Brothers, R.N., 1988. Petrology of Rumble seamounts, southern Kermadec Ridge, southwest Pacific. Bull. Volcanol. 50, 139–147.
Smith, I.E.M., Brothers, R.N., Muiruri, F.G., Browne, P.R.L., 1988. The geochemistry of rock and water samples from Curtis Island volcano, Kermadec group, southwest Pacific. J. Volcanol. Geotherm. Res. 34, 233–240.
Smith, I.E.M., Stewart, R.B., Price, R.C., 2003a. The petrology of a large intra-oceanic silicic eruption: the Sandy Bay Tephra, Kermadec arc, Southwest Pacific. J. Volcanol. Geotherm. Res. 124, 173–194.
Smith, I.E.M., Worthington, T.J., Stewart, R.B., Price, R.C., Gamble, J.A., 2003b. Felsic volcanism in the Kermadec arc, SW Pacific: crustal recycling in an oceanic setting. In: Larter, R.D., Leat, P.T. (Eds.), Intra-Oceanic Subduction Systems: Tectonic and Magmatic Processes, Geol. Soc. London Spec. Pub., vol. 219, pp. 99–118.
Tamura, Y., Tatsumi, Y., 2002. Remelting of an andesitic crust as a possible origin of rhyolitic magma in oceanic arcs: an example from the Izu-Bonin arc. J. Petrol. 43, 1029–1047.
Thouret, J.-C., 1999. Volcanic geomorphology—an overview. Earth Sci. Rev. 47, 95–131.
Turner, S., Hawkesworth, C., Rogers, N., Bartlett, J., Worthington, T., Hergt, J., Pearce, J., Smith, I., 1997. ^{238}U–^{230}Th disequilibria, magma petrogenesis, and flux rates, beneath the depleted Tonga-Kermadec island arc. Geochim. Cosmo. Acta 61, 4855–4884.
Van Wyk de Vries, B., Francis, P.W., 1997. Catastrophic collapse at stratovolcanoes induced by gradual volcano spreading. Nature 387, 387–390.
Wilson, C.J.N., Houghton, B.F., McWillimas, M.O., Lanphere, M.A., Weaver, S.D., Briggs, R.M., 1995. Volcanic and structural evolution of Taupo Volcanic Zone, New Zealand: a review. J. Volcanol. Geotherm. Res. 68, 1–28.
Woodhead, J.D., 1988. The origin of geochemical variations in Mariana lavas: a general model for petrogenesis in intra-oceanic island arcs? J. Petrol. 29, 805–830.
Worthington, T.J., 1998. Geology and petrology of Raoul Volcano: magma genesis and fractionation processes beneath the Tonga–Kermadec arc. PhD thesis, University of Auckland.
Worthington, T.J., Gregory, M.R., Bondarenko, V., 1999. The Denham caldera on Raoul volcano: dacitic volcanism in the Tonga–Kermadec arc. J. Volcanol. Geotherm. Res. 90, 29–48.
Wright, I.C., 1996. Volcaniclastic processes on modern submarine arc stratovolcanoes: sidescan and photographic evidence from the Rumble IV and V volcanoes, Southern Kermadec Arc (SW Pacific). Mar. Geol. 136, 21–39.
Wright, I.C., 1997. Morphology and evolution of the remnant Colville and active Kermadec arc ridges south of 33°30′ S. Mar. Geophys. Res. 19, 177–193.
Wright, I.C., Gamble, J.A., 1999. Southern Kermadec submarine arc caldera volcanoes (SW Pacific): caldera formation by effusive and pyroclastic eruption. Mar. Geol. 161, 207–227.
Wright, I.C., Parson, L.M., Gamble, J.A., 1996. Evolution and interaction of migrating cross-arc volcanism and backarc rifting: An example from the southern Havre Trough (35°20′–37° S). J. Geophys. Res. 101, 22,071–22,086.
Wright, I.C., de Ronde, C.E.J., Faure, K., Gamble, J.A., 1998. Discovery of hydrothermal sulfide mineralisation from southern Kermadec arc volcanoes (SW Pacific). Earth Planet. Sci. Lett. 164, 335–343.
Wright, I.C., Stoffers, P., Hannington, M., de Ronde, C.E.J., Herzig, P., Smith, I.E.M., Browne, P.R.L., 2002. Towed-camera investigations of shallow–intermediate water-depth submarine stratovolcanoes of the southern Kermadec arc. Mar. Geol. 185, 207–218.

Wright, I.C., Gamble, J.A., Shane, P.A., 2003. Submarine, silicic volcanism of the Healy caldera, southern Kermadec arc (SW Pacific): I. Volcanology and eruption mechanisms. Bull. Volcanol. 65, 15–29.

Yuasa, M., Murakami, F., Saito, E., Watanabe, K., 1991. Submarine topography of seamounts on the volcanic front of the Izu-Ogasawara (Bonin) arc. Bull. Geol. Surv. Japan 42, 703–743.

Zellmer, K.E., Taylor, B., 2001. A three-plate kinematic model for Lau Basin opening. Geochem. Geophys. Geosyst. 2. doi:10.1029/2000GC000106.